

1 **Variability of phenology and fluxes of water and carbon**
2 **with observed and simulated soil moisture in the Ent**
3 **Terrestrial Biosphere Model (Ent TBM version 1.0.1.0.0)**

4
5 **Y. Kim^{1,2}, P. R. Moorcroft³, I. Aleinov⁴, M. J. Puma⁴, N. Y. Kiang²**

6 [1]{Department of Civil and Environmental Engineering, Yonsei University, Seoul 120-749,
7 Korea}

8 [2]{NASA Goddard Institute for Space Studies, New York, NY 10025, USA}

9 [3]{Department of Organismic and Evolutionary Biology, Harvard University, Cambridge,
10 MA 02138, USA}

11 [4]{Center for Climate Systems Research, Columbia University, New York, NY 10025,
12 USA}

13 Correspondence to: Yeonjoo Kim (yeonjoo.kim@yonsei.ac.kr)

14
15 **Abstract**

16 The Ent Terrestrial Biosphere Model (Ent TBM) is a mixed-canopy dynamic global
17 vegetation model developed specifically for coupling with land surface hydrology and general
18 circulation models (GCMs). This study describes the leaf phenology submodel implemented
19 in the Ent TBM version 1.0.1.0.0, coupled to the carbon allocation scheme of the Ecosystem
20 Demography (ED) model. The phenology submodel adopts a combination of responses to
21 temperature (growing degree days and frost-hardening), soil moisture (linearity of stress with
22 relative saturation), and radiation (light length). Growth of leaves, sapwood, fine roots, stem
23 wood, and coarse roots is updated on a daily basis. We evaluate the performance in
24 reproducing observed leaf seasonal growth as well as water and carbon fluxes for four plant
25 functional types at five Fluxnet sites, with both observed and prognostic hydrology, and
26 observed and prognostic seasonal leaf area index. The phenology submodel is able to capture
27 the timing and magnitude of leafout and senescence for temperate broadleaf deciduous forest
28 (Harvard Forest and Morgan-Monroe State Forest, US), C3 annual grassland (Vaira Ranch,

1 US), and California oak savanna (Tonzi Ranch, US). For evergreen needleleaf forest
2 (Hyytiälä, Finland), the phenology submodel captures the effect of frost-hardening of
3 photosynthetic capacity on seasonal fluxes and leaf area. We address the importance of
4 customizing parameter sets of vegetation soil moisture stress response to the particular land
5 surface hydrology scheme. We identify model deficiencies that reveal important dynamics
6 and parameter needs.

7

8 **1 Introduction**

9 Phenological timing remains a major weakness of land surface dynamic global vegetation
10 models (DGVMs) that are coupled to general circulation models (GCMs), and a primary
11 cause of uncertainty in predicting the trajectory of global atmospheric CO₂ (Friedlingstein et
12 al. 2006, Friedlingstein et al. 2014). Seasonal variation of vegetation foliage, i.e., leaf
13 phenology, determines the timing and duration of the photosynthetically active canopy,
14 influencing stomatal activity, surface albedo and surface roughness (Jolly and Running 2004).
15 Thus, it plays a crucial role in the exchange of water, energy and carbon between land and the
16 overlying atmosphere. Numerous observations show that the interannual variability of
17 transpiration and gross primary productivity is associated with timings of leaf-out and leaf
18 senescence across ecosystem types (Goulden et al., 1996). Light-controlled leaf phenology is
19 suggested as a key controlling factor responsible for increasing carbon and water fluxes from
20 land to the atmosphere during the dry season in the Amazon rainforests (Hutyra et al. 2007,
21 Kim et al. 2012). Phenology is also tightly connected to other ecosystem processes, exerting
22 strong controls on the amount of assimilated carbon that is subsequently utilized for plant
23 growth and reproduction. Kramer (2000) showed that phenology could have effects on the
24 species composition of temperate-zone deciduous forests and the geographical distribution of
25 species since difference in phenological response leads to difference in light availability and
26 therefore growth in mixed species stands. Given the strong interactions between phenology
27 and other land surface and ecosystem processes, phenology affects both weather and climate.
28 Seasonal variation in vegetation characteristics have been shown to significantly influence
29 summer precipitation and temperature in the U.S. (Dirmeyer 1994, Xue et al. 1996), and
30 enhance or weaken the feedbacks between soil moisture and precipitation in the continental
31 interior of North America depending on soil moisture conditions and season (Kim and Wang
32 2007). Levis and Bonan (2004) demonstrated that the coupling between phenology and the

1 atmosphere is critical for models to capture seasonal weather evolution. Tightly linked to
2 phenology, plant carbon allocation, that is, distribution of assimilated carbon among the plant
3 parts, also responds to environmental and climate conditions (such as increases in air
4 temperature, changes in precipitation patterns and elevated atmospheric CO₂ concentration).
5 For example, Pumpanen et al. (2012) observed that root biomass and the rate of
6 photosynthesis for silver birch, Norway spruce and Scots pine seedlings increase with higher
7 soil temperature, yet a simultaneous increase in both photosynthesis and respiration rates
8 results in no change in net CO₂ exchange and total seedling biomass.

9 Terrestrial biosphere models (TBMs) or Dynamic Global Vegetation Models (DGVMs) have
10 been developed and coupled to General Circulation Models (GCMs) (e.g., Foley et al. 1996,
11 Cox 2001, Sitch et al. 2003, Bonan and Levis 2006, Dunne et al. 2013), to account for
12 biophysical and biogeochemical processes and sometimes biogeography, allowing prediction
13 of transient terrestrial ecosystem interactions with climate (Cramer et al. 2001, Friedlingstein
14 et al. 2006). Thus the active role of vegetation phenology can be incorporated into climate
15 modeling. TBMs have been parameterized and evaluated on the basis of local, regional, or
16 global scale studies. It has become common to evaluate the models at the individual field
17 scale at sites with eddy flux measurements and detailed ground data (e.g., Delire and Foley
18 1999, Arora and Boer 2005, Krinner et al. 2005, Kucharik et al. 2006, Friend et al. 2007,
19 Stöckli et al. 2008, Bonan et al. 2011). Still, parameterizations for vegetation processes (such
20 as phenology and carbon allocation) implemented in TBMs are often limited to local-scale
21 derivations due to the lack of high-quality global scale observations of vegetation structure
22 and function together with meteorological conditions and mechanistic understanding free of
23 local effects.

24 Prognostic phenology models have been developed to predict phenological response of
25 vegetation to climate based on empirical evidence, as a mechanistic, process-based treatment
26 is still not fully realizable with current understanding (Sala et al. 2012). The more commonly
27 used climatic rule-based approach accounts for cues by temperature, soil moisture, and day
28 length cues to phenology, to predict leaf-on and leaf-off, with these controls often
29 represented as a cumulative functions of one or several climate variables that reach an
30 empirically defined threshold (White et al. 1997). Another approach is based on plant carbon
31 status (Bonan et al. 2003), and predicts leaf-out and senescence on the basis of potential

1 positive carbon assimilation, which is in turn is affected by temperature, moisture, and
2 sometimes nutrient conditions.

3 All of the above approaches require empirical parameterization of the responses to climate,
4 and a model scheme that is independent of PFT or geographical variation is still a research
5 goal. Jolly et al. (2005) have proposed a very simple and promising bioclimatic Growing
6 Season Index (GSI) for phenology based on linear relations to minimum temperature,
7 photoperiod, and vapor pressure deficit (VPD, as a proxy for soil moisture), which seems to
8 perform well compared to satellite observations at diverse sites. However, it performs less
9 well for arid systems for which VPD may not be a good indicator of available deep soil
10 moisture, and it is not able to capture any seasonal moisture or light sensitivity that has been
11 observed in tropical evergreen forests (Stockli et al. 2011). Forkel et al. (2014) adopted the
12 concept of GSI but used the soil water availability instead of VPD for water limiting function.
13 Phenology depends not only on atmospheric water demand but also on water supply from soil
14 moisture as Migliavacca et al. (2011) have shown that GSI performed better when using a soil
15 moisture limiting function instead of the VPD limiting function. Recently, Caldararu et al.
16 (2014) introduced a promising optimality approach based on the hypothesis that phenology is
17 a strategy for optimal leaf area index, rather than explicit carbon exchange, driven by canopy-
18 level demand for – and constrained by availability of -- light and water, limited by leaf aging.
19 They fitted the model to satellite observations of LAI and demonstrated its capability to
20 reproduce phenological patterns for different vegetation types over the globe within 8-16 days
21 of observations. Top-down optimality approaches such as this may indeed be the smart way
22 for global scale models way to capture the strategic behaviors inherent in phenology in lieu of
23 mechanistic understanding at the leaf or molecular level; the next step remains to couple them
24 with explicit carbon exchange and allocation.

25 In this study, we perform a site-based model evaluation study for the Ent¹ Terrestrial
26 Biosphere Model's (Ent TBM version 1.0.1.0.0²) coupled phenology/growth schemes. This

¹ Ent is not an acronym but the name of a sentient species of tree in J.R.R. Tolkien's fantasy novels, *The Lord of the Rings*.

² Enumeration is in order for different levels of dynamics and different physics versions available for each of these. In order, the digits denote:

1) Primary biophysics (leaf, soil biogeochemistry) and base release version (1: leaf biophysics as described in Schmidt et al. 2014; soil biogeochemistry described in this paper).

2) Canopy radiative transfer (0: two-stream as described in Schmidt et al. 2014; 1: ACTS

1 evaluation is a necessary task before introducing prognostic phenology into global
2 simulations coupled with a GCM atmosphere in order to enable modeling of interactive
3 phenology and climate. We do not offer yet a new paradigm, but the phenological timing
4 schemes provide a synthesis of approaches in the literature to capture the full combination of
5 climatological drivers thus far known to be essential for each type of phenology, and
6 introduce some new functional representations to do so. These are coupled to growth
7 algorithms from the Ecosystem Demography (ED) model (Moorcroft et al. 2001) that
8 account for both the geometric and mass allometry of plant functional types.

9 In this paper, we describe the Ent TBM's phenology and allometry scheme coupled to the ED
10 carbon allocation scheme, and evaluate their performance at Fluxnet sites (Baldocchi et al.
11 2001), focusing on seasonal and inter-annual variations of LAI and carbon and water fluxes.
12 We compare site simulations using both observed soil moisture and that modeled by a land
13 surface hydrology model coupled to the Ent TBM. The phenology schemes synthesize
14 several observational data sets, combining both climate responses and a carbon balance
15 approach, described in detail below. Here we evaluate the performance for temperate
16 broadleaf deciduous forest, C3 annual grassland, evergreen needleleaf forest, and tree/grass
17 savanna (mixed drought deciduous broadleaf and C3 annual grassland). Through these
18 evaluations, we are interested in quantifying the accuracy of the current model at the site
19 level, and we identify ecosystem processes needing further improvement, with regard to both
20 plant growth dynamics and the representation of soil moisture.

21

22 **2 Model descriptions**

23 **2.1 Land Surface Model (LSM) of the NASA GISS GCM**

24 The Ent TBM can be run with observed soil moisture and temperature, and canopy
25 temperature inferred from eddy flux measurements of sensible heat fluxes, or, given
26 precipitation and air temperature, it can obtain modeled soil moisture, temperature, and

model (Ni-Meister et al. 2010; Yang et al., 2010);

3) Leaf phenology (0: prescribed from satellite data; 1: prognostic, this paper);

4) Carbon allocation/growth (0: allocation with prognostic phenology, without structural growth, this paper; 1: allocation with structural growth).

5) Ecosystem dynamics (0: none; 1: Ecosystem Demography scheme).

1 canopy temperature, if run coupled to a land surface hydrology model. For the coupled mode,
2 we use the land model of the National Aeronautics and Space Administration (NASA)
3 Goddard Institute for Space Studies (GISS) general circulation model (GCM) (Schmidt et al.
4 2006). The NASA GISS GCM land hydrology consists of six soil layers down to 3.5 m depth
5 based on Rosenweig and Abramopoulos (1997), with updates described in Schmidt et al.
6 (2006; 2014). The land surface model (LSM) computes the fluxes of heat and water vapor to
7 the atmosphere, and the energy balance of the soil and vegetation canopy. Surface runoff is
8 calculated based on saturation and infiltration capacity of the upper soil layer. The
9 underground runoff is computed according to a formulation of Abramopoulos et al. (1988),
10 which takes into account the average slope and the density of underground sinks in the cell.
11 When running the Ent TBM coupled to the GISS LSM, soil physics parameters are taken
12 from the land surface mapped datasets of the GISS LSM.

13 **2.2 Ent Terrestrial Biosphere Model (Ent TBM)**

14 The Ent TBM is a standalone model developed specifically for coupling the fluxes of water,
15 energy, carbon, and other trace gases between LSMs and GCMs. It is structured like the ED
16 model (Moorcroft et al. 2001) for simulating competition in mixed canopies and disturbance
17 dynamics by representing vertical canopy structure through ensemble cohorts of identical
18 individuals, and horizontal heterogeneity via subgrid patch communities. The specifications
19 of canopy geometry and allometry of biomass pools are consistent with individual ellipsoidal
20 crown geometry that is integrated with the coupled phenology/growth model. This paper
21 presents simulations of seasonal variation in leaf area and mass and in fluxes of CO₂, water
22 vapor, and sensible and latent heat of both transpiration and ground evaporation.

23 Fig. 1 shows a conceptual diagram of the Ent model, and how it is coupled with a GCM (or
24 off-line meteorological forcings) and an LSM. Ent's biophysics modules operate at the
25 physical time step of the GCM or LSM. The photosynthetic uptake of carbon utilizes the
26 well-known photosynthesis model of Farquhar et al. (1980) and Farquhar and von Caemmerer
27 (1982) coupled with the stomatal conductance model of Ball and Berry (Ball et al. 1987),
28 while Ent uses its own cubic solution for these coupled equations. Canopy radiative transfer
29 is optionally modeled as in Friend and Kiang (2006) for homogeneous canopies, or as in Ni-
30 Meister et al. (2010) and Yang et al. (2010) for clumped canopies. In this paper, in lieu of
31 detailed site allometric and canopy structure data, we utilize the homogeneous canopy
32 radiative transfer scheme. Carbon uptake is accumulated over a day so that carbon allocation

1 to growth, phenological behavior, and mortality are updated once per day. An individual
2 plant has distinct biomass pools, including a "labile" or carbohydrate reserve pool into which
3 photosynthetic uptake and retranslocated carbon are accumulated; "active" pools consisting of
4 foliage, fine roots, a reproductive pool, and, for woody plants, live sapwood, and "dead" pools
5 consisting of dead stem wood and coarse roots. Autotrophic respiration is the sum of
6 maintenance respiration as function of biomass and temperature, "activity growth respiration"
7 as function of gross assimilation, and tissue growth respiration as a function of amount of new
8 growth.

9 Ent takes its meteorological drivers and hydrological balance at the grid cell or catchment
10 zone scale of the LSM and subgrid heterogeneity is represented as dynamic patches of
11 vegetation communities, comprised of cohorts of plants that are ensembles of identical
12 individuals (patch and community dynamics are not part of this study). The biomass pools
13 and geometry of an individual woody plant are illustrated in Fig. 2 Canopy conductances
14 from each patch are summed to the grid cell or catchment zone level to couple with the
15 atmosphere. Also, root density vertical profile distributions in Ent are used to calculate a
16 depth-weighted average of soil moisture stress. These profiles are a modification of those in
17 Rosenzweig and Abramopoulos (1997), with details given in the Appendix A.

18 The Ent TBM is designed to support a flexible number of plant functional types (PFTs). A
19 parameter set for 17 PFTs has been developed, as listed in Table 1; however, we note that
20 only a subset of these PFTs is evaluated here according to data availability, and the others
21 must be approximated from the available similar types and theoretical/empirical relations
22 from the literature. Following the rationale first advocated by Defries et al.(1995) and
23 adopted by all vegetation models since then to varying degrees, Ent's PFTs distinguish
24 photosynthetic pathway (C3 and C4), phenological type (evergreen, cold deciduous and
25 drought deciduous), leaf type (broadleaf and needleleaf), growth form (tree, shrub, and
26 herbaceous), and cultivated (herb crops). In addition, to better capture community dynamics
27 in mixed canopies, if parameter sets are provided, Ent has the capability to distinguish early
28 and late successional species through differences in leaf life span, following the approach of
29 the ED model (Moorcroft et al. 2001), which is based on leaf physiological relations found in
30 Reich et al. (2007).

31 To capture total net carbon fluxes, the Ent TBM incorporates the code implementation of
32 CASA' from the Community Land Model 3.0 (CLM 3.0, Randerson et al. 2009; Doney et al.,

1 2006; code kindly supplied by Jasmin John), which is based on the Carnegie-Ames-Stanford-
2 Approach of Potter et al. (1993). For the Ent TBM, the CASA' temperature and soil moisture
3 responses of respiration were replaced with functions derived from new fits to field data of
4 Del Grosso et al. (2005). Details are provided in Appendix B.

5 As mentioned earlier, the Ent TBM can be run in several different modes of coupling: (1) a
6 stand-alone mode when the meteorological (e.g., radiation, precipitation, air temperature, air
7 pressure, humidity and wind) and land conditions (e.g., soil moisture and soil temperature,
8 and canopy temperature) are provided ("Ent-standalone"), (2) a mode coupled with a LSM for
9 prognostic soil moisture and temperature given meteorological forcings ("Ent-LSM"), and (3)
10 a fully coupled mode with an atmospheric GCM. Ent-standalone and Ent-LSM modes can be
11 used for site-specific simulations or regional/global simulations using observed
12 meteorological and soil moisture data.

13 The Ent TBM can also be run with different levels of vegetation dynamics turned on or off.
14 In a biophysics-only mode, canopy structure and leaf area are prescribed, to simulate only
15 fluxes of water vapor, carbon dioxide, and other trace gases. In an "active biomass"
16 phenology-only mode, canopy stem structure is prescribed and static, while seasonal leaf and
17 fine root dynamics are prognostic, and carbon that would have been allocated to stem and
18 coarse root growth instead is allocated to litter. In a phenology-woody growth mode, in
19 addition to leaf phenology, stem and coarse root growth are also enabled. In an ecosystem-
20 dynamics mode, mortality and disturbance ensure that plants cannot grow indefinitely and are
21 subject to succession and cover change (ecosystem dynamics are not covered in this paper).

22 **2.3 Plant growth submodel**

23 The plant growth submodel integrates phenological timing and allocation of carbon to growth
24 and litter fluxes (background litterfall and seasonal), and respiration fluxes tied to tissue
25 growth. The phenology scheme determines the phenological status of plants based on various
26 environmental and climate rules studies, which determine budburst, frost-hardening, and
27 senescence according to the phenological types of plants such as drought-deciduousness and
28 cold-deciduousness. The carbon fixed over the course of each day from photosynthesis is
29 accumulated and placed into a labile carbohydrate reserve pool. Carbon from the labile pool is
30 then allocated once per day into different plant pools of foliage, sapwood, heartwood, fine
31 root and coarse root as well as a reproductive pool according to empirical allometric

1 relationships and leaf phenological status. In addition, tissue lost to background litter fluxes
2 is replenished, and respiration fluxes are produced from growth of any tissue. A portion of
3 litterfall is retranslocated back to the labile pool.

4 In the Ent TBM, the carbon allocation scheme takes a traditional approach of ‘static
5 allocation’, based on fixed allometric relationships between different pools. Adopted from
6 approaches of the ED models (Moorcroft et al. 2001, Medvigy et al. 2009). Appendix C
7 provides the descriptions of the ED allocation scheme, which treats “active” and “dead”
8 biomass pools as bulk sinks, with modifications for Ent. We identified some deficiencies of
9 the ED allocation scheme, and suggest future work for improvement in Section 5. Also note
10 that Appendix D provides the biophysical, phenological and allocation parameter values used
11 in this study.

12 Full prognostic growth entails growth of woody structure and the size of woody plants, which
13 would require in addition full mortality and establishment dynamics so that there is not
14 unlimited growth; these population and community dynamics will be presented in future
15 papers. This study focuses on the “active biomass” performance of Ent given seasonal
16 phenology, keeping woody structure static, allocating the amount that would have gone to
17 growth instead to litterfall.

18 **2.4 Phenology**

19 The phenology scheme in the Ent TBM provides a synthesis, and combines the climatic rule-
20 based approach and carbon balance for deciduous plants to determine the timings and rates of
21 leaf out and leaf senescence by integrating several different modeling studies. We present a
22 diversity of PFTs, adding those with known behaviors that depart from common
23 representations of cold, drought, or light responses. While globally applicable
24 parameterizations of climate rule-based phenology may still be elusive, where available in the
25 literature, we draw from wide surveys that attempt to extrapolate to the global scale.

26 For deciduous plants, we use parameterizations by Botta et al. (2000). With growing degree
27 day (GDD) and chilling requirement, they examined the possibility of extrapolating existing
28 local models for leaf onset date to the global scale by retrieving leaf onset dates from the
29 NOAA/AVHRR satellite normalized difference vegetation index (NDVI). They identified
30 appropriate leaf onset date models and estimated their parameters for each biome, which are
31 implemented in other ecosystem models (Medvigy et al. 2008). The importance of a chilling

1 requirement is confirmed by Richardson et al. (2012), who conducted an inter-comparison of
2 phenology predictions of eleven TBMs (and three biophysics models with prescribed
3 phenology) at five deciduous broadleaf and five evergreen needleleaf Fluxnet sites. They
4 found that, for deciduous forests, the models consistently predicted an earlier onset of the
5 growing season and later fall senescence than observed; meanwhile, most models under-
6 predicted the magnitude of peak GDD sums, while those that explicitly or implicitly included
7 a chilling requirement did relatively well in capturing the onset of LAI and GPP for deciduous
8 and evergreen forests, compared to simple temperature threshold schemes. For drought
9 deciduous trees and grasses, we also make use of parameterizations of White et al. (1997)
10 who developed a regional phenology model for the US, predicting timings of leaf onset and
11 offset based on the satellite NDVI at the 20 km resolution. Their prediction errors are ~1
12 week, and maximum expected errors are 10-14 days.

13 For evergreen vegetation, the Ent TBM includes frost-hardening for boreal evergreen plants.
14 The frost-hardening (also called winter cold-hardening) involves physiological changes to
15 protect the plant from chilling injury and freezing injury, leading to a downgrading of leaf
16 photosynthetic capacity as well as tissue turnover and respiration. Coniferous vegetation in
17 the boreal zone has a clear annual cycle of photosynthetic activity, with photosynthesis low or
18 zero during the winter, increasing during the spring, peaking during the summer, and
19 decreasing during the fall. While part of the cycle is due to direct responses to PAR and air
20 temperature, the inherent photosynthetic capacity of needles also changes (Makela et al.
21 2004). Therefore, the models that do not account for cold-hardening and de-hardening will
22 over-predict the uptake of carbon by photosynthesis for boreal systems during the late fall
23 through early spring. This study implements a frost-hardening algorithm based on Hanninen
24 and Kramer (2007), Makela et al. (2006) and Repo et al. (1990), who developed a model of
25 the frost-hardiness of the stems of Scots pine seedlings. Below we describe the explicit model
26 functions reflecting our choices based on the literature above.

27

28 **2.4.1 Phenology Model Climate Cue Framework**

29 In the Ent TBM, several “phenological factors”, φ_x , as well as physiological stress factors, β_x ,
30 are calculated for seasonal environmental cues from various climate measures x . These
31 include air and soil temperature history (cumulative number of growing degree days and of

1 chilling days), day-length and soil moisture. The phenological factors control the allocation
 2 of assimilated carbon, while the physiological stress factors affect the efficiency of carbon
 3 uptake, and all range from 0 to 1 on a daily basis. Different rules apply to the different PFTs,
 4 according to phenotype (woody plant cold-deciduous, *cd*; drought-deciduous; *dd*, evergreen,
 5 *ev*; tropical radiation phenology, *tr*; and cold deciduous herbs, *c*, whether annual or
 6 perennial). The phenological factor controls the timing and rate of carbon transfer between the
 7 labile and active carbon pools and hence the seasonal variation in leaf area index (LAI), fine
 8 roots, and sapwood.

9 Furthermore, the Ent TBM determines “phenological status”, *Phenostatus_p*, where *p* is the
 10 phenotype, which identifies phenologically different seasons. For plants with seasonal leaf-
 11 out and senescence, *Phenostatus_p* is 1 for the leaf-off season, 2 for the leaf-up period, 3 for the
 12 peak foliage period, and 4 for the senescent period. The trend in length of day (*ld*) is used to
 13 determine which season it is, or, rather, which half of the year it is. If day length is
 14 decreasing, then it is the latter half of the year, and “fall” may be allowed to commence,
 15 depending on other climate variables of phenological factors. Below we itemize these
 16 variables and equations in the Ent phenology scheme.

17 **2.4.2 Cold deciduous woody plants**

18 During the winter, the phenological status of cold-deciduous trees and shrubs, *Phenostatus_{cd}*,
 19 is 1, for no foliage. Leaf-out (*Phenostatus_{cd}*=2) occurs once the cumulative number of
 20 growing degree days (*GDD*) exceeds its critical number (*GDD_{crit}*), which is determined with a
 21 function of cumulative number of chilling days (*NCD*) (Botta et al. 2000). Following Kim and
 22 Wang (2005), the 10-day running average of air temperature (*T₁₀*) difference from the base
 23 temperature (*T_{base}*) of 5°C is used to calculate *GDD* and *NCD* on a daily basis as follows:

$$24 \quad GDD(t) = GDD(t - 1) + \max(0, T_{10} - T_{base}) \quad (1)$$

$$25 \quad NCD(t) = NCD(t - 1) + 1 \quad \text{if } T_{10} < T_{base}. \quad (2)$$

26 where *t* is time in days. *GDD* and *NCD* are reset to be zero at the beginning of the winter
 27 season (when *Phenostatus_{cd}* switches from 4 to 1). The function for *GDD_{crit}* is expressed as
 28 follows:

$$29 \quad GDD_{crit} = GDD_{intercept} + GCC_{slope} e^{(NCD_{multi} \cdot NCD)} \quad (3)$$

30 where the constant values of *GDD_{intercept}*, *GDD_{slope}* and *NCD_{multi}* are provided in Table 2.

1 Once leaf-out starts, trees take a number of degree days (GDD_{length}) to reach the
 2 phenologically unconstrained status (Foley et al. 1996). We introduce an approach to scale
 3 the departure of GDD from GDD_{crit} with GDD_{length} , and to have a phenology factor, φ_{GDD} ,
 4 that ranges from 0 to 1:

$$5 \quad \varphi_{GDD} = \begin{cases} \frac{GDD - GDD_{crit}}{GDD_{length}} & \text{when } GDD > GDD_{crit}, \\ 0 & \text{otherwise.} \end{cases} \quad (4)$$

6 When $\varphi_{GDD}=1$, then the $Phenostatus_{cd}$ switches to 3, peak foliage. Full or peak foliage may
 7 also occur when carbon allocation to foliage reaches the maximum supported by the available
 8 sapwood.

9 Fall senescence ($Phenostatus_{cd}=4$) can commence in response to shortening day length
 10 (“fall”) and decreased air temperature, in a modification of White et al. (1997) and Jolly et al.
 11 (2005). Leaves start dropping once air temperature or day length decreases down to threshold
 12 values (i.e., T_{max} and ld_{max}) proportionally to the temperature decreases in the fall as in Eq. (5).
 13 Full senescence finally occurs when air temperature or day length decrease further down to
 14 the minimum thresholds (i.e., T_{min} and ld_{min}). The phenological factor with respect to air
 15 temperature, φ_T , is:

$$16 \quad \varphi_T = \begin{cases} \min\left(1, \frac{T_{10} - T_{min}}{T_{max} - T_{min}}, \frac{ld - ld_{min}}{ld_{max} - ld_{min}}\right) & \text{when } T_{10} < T_{max} \text{ or } ld < ld_{max}, \\ 0 & \text{otherwise.} \end{cases} \quad (5)$$

17 T_{max} , T_{min} , ld_{max} and ld_{min} are constants, with values provided with references in Table 2.

18 **2.4.3 Cold deciduous herbaceous plants**

19 Phenological status of cold-deciduous (annual or perennial) herbaceous plants is well
 20 captured with functions based on soil temperature (TS), while that of cold-deciduous woody
 21 plants is with air temperature (White et al. 1997). Similarly to Eqs. 1 and 4 for cold
 22 deciduous trees, the soil growing degree days ($SGDD$) of soil temperature (TS_{10}) is calculated
 23 with the base temperature constant (TS_{base}) of 0°C. Grasses generate leaves once $SGDD$
 24 exceeds its PFT-dependent critical number ($SGDD_{crit}$) and the phenology factor for $SGDD$,
 25 φ_{SGDD} , becomes 1 or greater, as follows:

$$26 \quad \varphi_{SGDD} = \begin{cases} \frac{SGDD - SGDD_{crit}}{SGDD_{length}} & \text{when } SGDD > SGDD_{crit}, \\ 0 & \text{otherwise.} \end{cases} \quad (6)$$

1 While White et al. (1997) derived $SGDD_{crit}$ as a logistic function of mean annual soil
 2 temperature, here we simplify it with three different numbers for different grass types as
 3 provided in Table 2. The parameters for φ_{SGDD} were fit to observations at Barrow, Alaska, for
 4 arctic C3 grass; the values for C3 and C4 grasses are drawn from White et al. (1997).

5 Grasses begin fall senescence in response to decreased soil temperature. Leaves start
 6 dropping once soil temperature decreases down to a given threshold, TS_{max} ; grasses complete
 7 senescence when soil temperature decreases further down to the critical threshold, TS_{min} :

$$8 \quad \varphi_{TS} = \begin{cases} \min\left(1, \frac{TS_{10} - TS_{min}}{TS_{max} - TS_{min}}\right) & \text{when } TS_{10} < TS_{max}, \\ 0 & \text{otherwise.} \end{cases} \quad (7)$$

9 See Table 2 for constant values of TS_{max} and TS_{min} .

10 **2.4.4 Drought deciduous woody and herbaceous plants**

11 Drought deciduousness depends on available soil water for the plant. In the model, it is
 12 determined based on a 10-day running average of the physical time step (~half-hourly) plant
 13 water stress factor β . This factor is the same used to scale stomatal conductance for water
 14 stress, and is determined by a linear response between PFT-dependent critical relative soil
 15 moisture (volumetric soil moisture/saturated volume) points for the plant, at which water
 16 stress begins, s_* , and at which wilting occurs, s_{wilt} , (Rodriguez-Iturbe et al. 2001):

$$17 \quad \beta = \frac{s - s_{wilt}}{s_* - s_{wilt}}. \quad (8)$$

18 $\beta=1$ when the plant is unstressed, and $\beta=0$ at the wilting point. For 6 soil layers in the LSM,
 19 β is calculated for the soil moisture in each layer, and averaged weighted by layer thickness
 20 and relative root mass fraction, giving the overall β experienced by the plant.

21 The phenological factor for water stress, φ_β , is determined by a linear response to the 10-day
 22 running average (Foley et al. 1996) of water stress, β_{10} , to β_{max} and β_{min} , which represent
 23 similarly 10-day running averages of water stress experienced before the onset of drought-
 24 induced senescence and at full senescence:

$$25 \quad \varphi_\beta = \max\left(0, \left(\frac{\beta_{10} - \beta_{min}}{\beta_{max} - \beta_{min}}\right)^{\beta_{resis}}\right) \quad (9)$$

26 When β_{10} goes below a minimum (β_{min}), plants completely senesce in response to drought
 27 ($\varphi=0$); when β_{10} is above a maximum (β_{max}), plants do not experience drought ($\varphi=1$); when

1 β_{I0} is between β_{min} and β_{max} , the sensitivity of plants to water availability is controlled by the
2 resistance factor (β_{resis}). The values of s^* , s_{wilt} , β_{min} , β_{max} and β_{resis} are provided in Table 2.

3 The leaf-on cue for drought deciduous trees is the same as that for cold-deciduous
4 trees, while for grasses the cue is sufficient soil moisture.

5 **2.4.5 Frost-hardening in evergreen cold-climate plants**

6 Boreal plants undergo winter frost-hardening, which involves physiological changes to
7 protect the plant from chilling injury and freezing injury. Following Repo et al. (1990), the
8 state of frost hardiness S_h ($^{\circ}\text{C}$) is modeled as follows:

$$9 \frac{dS_h}{dt} = \frac{1}{\tau} [(a \cdot T_{10} + b) - S_h]. \quad (10)$$

10 where τ is a PFT-specific time constant, and the term $a \cdot T_{10} + b$ is the stationary frost hardiness,
11 where a and b are PFT-specific parameters for the linear relationship between stationary frost
12 hardiness and air temperature (Hanninen and Kramer 2007). S_h can be thought of as an
13 aggregated measure of the state of the physiological leaf processes that determine the
14 photosynthetic capacity (Makela et al. 2004).

15 The state of frost hardiness is then used to adjust the maximum photosynthetic capacity V_{cmax} ,
16 which is an approach similar to the work of Makela et al. (2006). However, we convert from
17 S_h to a dimensionless factor that can take values from 0 to 1. This frost hardiness factor
18 β_{frost} is expressed as:

$$19 \beta_{frost} = \frac{1}{S_{h,max}} (S_h - T_0). \quad (11)$$

20 where T_0 is a threshold value of cumulative mean temperature at which photosynthesis starts
21 and $S_{h,max}$ is the maximum value of S_h (see Table 2 for constants). We implement the first-
22 order Euler scheme to solve Eq. (10) and the resulting β_{frost} is used to adjust V_{cmax} .

23

24 **3 Experiments**

25 **3.1 Fluxnet sites**

26 The Ent TBM was evaluated at five Fluxnet sites, including Morgan Monroe State Forest,
27 Harvard Forest, the Vaira Ranch, the Tonzi Ranch and Hyytiala, as briefly mentioned above

1 (Table 3). From all sites, data from the flux tower systems were available. Meteorological
2 driver data include radiation, precipitation, air temperature, air pressure, humidity and wind,
3 used to drive the model. Soil moisture and temperature measurements were also used to
4 drive the Ent standalone simulations. Flux data includes net ecosystem exchange (NEE) and
5 evapotranspiration (ET), and were used to evaluate the simulation results. Among sites, data
6 availability, such as LAI, varied and suited different types of model simulations as described
7 in detail in the next section.

8 The Morgan Monroe State Forest (MMSF), located in Indiana, USA (Schmid et al., 2000)
9 (latitude: 39.32315°, longitude: -86.413139°) is an extensive managed temperate broadleaf
10 deciduous forest with a total area of 95.3 km². The area is covered primarily by a secondary
11 successional broadleaf forest within the maple-beech to oak-hickory transition zone of the
12 eastern deciduous forest, dominated by sugar maple and tulip poplar. LAI measurements at
13 5-14 day intervals during the growing season were available for 1998-2001.

14 Harvard Forest (latitude: 42.5313°, longitude: -72.1898°) is an eastern temperate mixed forest
15 dominated by deciduous trees. The area surrounding the flux tower is dominated by red oak
16 and red maple, with scattered stands of Eastern hemlock, white pine and red pine. About 1/3
17 of the existing red oaks were established prior to 1895, another 1/3 prior to 1930, and the rest
18 before 1940, and thus the stand is 75–110 years old (Urbanski et al., 2007). O'Keefe (2000)
19 provides the leaf phenology of Harvard Forest. The timings of spring leaf development and
20 fall leaf fall have been recorded for permanently tagged individuals in the field from 1991.
21 The leaf development and senescence data in percent of final leaf size have been used to
22 obtain 'observational' LAI based on the maximum LAI in the model, i.e., (observed LAI) =
23 (observed % of leaf development or fall) X (modeled maximum LAI).

24 The Vaira Ranch (latitude: 38.4066667°, longitude: -120.950733°) and Tonzi Ranch (latitude:
25 38.4316°, longitude: -120.9660°) in Ione, California, are located in an open grassland
26 ecosystem and an oak/grass savanna ecosystem, respectively, in a Mediterranean climate of
27 cool wet winters, and dry hot summers. The sites are less than 3 km apart. The grasses of both
28 sites are C3 annual species whose growing season is during the winter to spring wet periods.
29 Deciduous blue oaks dominate the savanna overstory of the Tonzi, with a growing season
30 overlapping the grasses during the spring and continuing through the summer drought. In
31 these sites, LAI measurements were available along the tower footprint for 2001 (Kiang,
32 2002).

1 Hyytiala (latitude: 61.8474150°, longitude: 24.294770°) in Finland is situated in needleleaf
2 evergreen forest dominated by *Pinus sylvestris* (Scots pine), in which the phenological
3 behavior of interest is frost-hardening. The climate is boreal. Flux measurements and soil
4 moisture and temperature are available. For seasonal LAI, we used the site investigator's
5 description of a constant minimum all-sided needleleaf LAI (75% of maximum) in January-
6 May, linear increase over June to its maximum of 3.9, remaining at the maximum LAI during
7 July-September, linear decline to its minimum in October, and a constant minimum LAI in
8 November-December (Kolari, personal communication, 2007).

9 **3.2 Experiment desgin**

10 We performed a series of numerical experiments with Ent in different model modes in order
11 to evaluate leaf seasonal dynamics, including leaf phenology and related water and carbon
12 fluxes. We performed simulations for each site with observed soil moisture (hereafter
13 denoted 'Ent' mode), and LSM modeled soil moisture ('LSM' mode); and with observed LAI
14 (without allocation of assimilated carbon to growth) ('oveg') and dynamically modeled LAI
15 (via carbon allocation) ('dveg'), giving four experiments, Ent-oveg, Ent-dveg, LSM-oveg,
16 and LSM-dveg (Table 4). In the biophysics-only mode, the observed LAI is prescribed and
17 related active carbon allocations are calculated according to that LAI. In the "active biomass"
18 phenology mode, the leaf phenology and active carbon allocation are dynamically simulated.
19 For MMSF and Harvard Forest, the model was forced with 6 and 9 years' worth of drivers,
20 respectively. In these two sites, continuous soil moisture measurements throughout the
21 rooting depth were not available, so only Ent-LSM simulations were performed. For Vaira,
22 Tonzi and Hyytiala, the model was forced with a year's worth of tower-measured
23 meteorological drivers as well as observed soil temperature and moisture.

24 For the Ent versus LSM simulations for annual grass phenology, it was necessary to tailor the
25 soil moisture stress parameterst to the different metrics of soil moisture. The phenological
26 timings of grasses depend on the soil moisture condition while an LSM-derived soil moisture
27 is a model-specific index of soil wetness, not a physical quantity that can be directly validated
28 with field measurements (Koster et al., 2009). The thresholds for the root water stress factor
29 (β in Eq. 8) that was used to model drought-deciduous behavior of grasses (volumetric soil
30 moisture at onset of stress and at wilting point) were derived from the observed soil moisture
31 and fluxes, such that these parameters were in a sense tuned to the site as well as to the type

1 of soil moisture measurement. In this study, we therefore tuned the parameters for LSM to
2 better capture the phenological behaviors.

3 For diagnostics for model performance, we examined observed monthly LAI, and monthly
4 sums of gross primary production (GPP), ecosystem respiration (R_E), net ecosystem
5 productivity ($NEP = GPP - R_E$) and total evapotranspiration (ET). For potentially water-
6 limited sites, we examined the modeled volumetric soil moisture and Ent's plant water stress
7 factor. For observed R_E , the values are inferred from nighttime respiration and its sensitivity
8 to soil temperature, while the modeled values result from both autotrophic and soil
9 respiration. Soil carbon as a driver of soil respiration was initialized from site measured soil
10 carbon, with litterfall from the model as inputs on a daily basis (soil carbon was not driven to
11 equilibrium).

12

13 **4 Results**

14 **4.1 Cold deciduous woody plants**

15 **4.1.1 Phenology**

16 We evaluated the model performance for cold deciduous woody plants at two sites, Morgan-
17 Monroe State Forest (MMSF) in Indiana, and Harvard Forest.

18 Figure 3 and Table 5 show the simulated variations of the phenological factor (ratio of LAI to
19 the maximum LAI of the year) in comparison to observations. First, it is clear that the gradual
20 nature of changes in LAI during spring and fall were not captured in the model. The
21 phenological factor serves as an on-/off cue between environmental thresholds, while growth
22 rate with the ED scheme is limited only by carbon availability, for which reserve carbon is
23 generally not limiting in trees (Sala et al. 2012) or in grass seeds (William Parton, pers.
24 communication). At both sites, the inter-annual variations of leaf-on timings in the spring
25 were better captured than those of the leaf-off timings in the fall. At Harvard Forest, the dates
26 with the elongation factor of 0.5 in spring showed a correlation coefficient (R) of 0.85 and a
27 root mean squared error (RMSE) of 3.00 days, while the dates with an elongation factor of 0.5
28 in fall showed R of 0.04 and an RMSE of 15.09 days.

1 **4.1.2 Fluxes**

2 In MMSF, the predicted NEP reasonably followed the observed NEP (Schmid et al. 2000,
3 Dragoni et al. 2007) with correlation coefficients ranging from 0.86 to 0.94, while the peak
4 NEP in summer was slightly underestimated compared to the observed (Fig. 4 and Table 6).
5 However, both GPP and R_E were both more extreme in the model compared to the Fluxnet
6 data product.

7 In Harvard Forest, the default simulations (LSM-dveg and LSM-oveg) showed
8 underestimated NEP compared to the flux tower observations due to simulated water stress
9 (Fig. 5). As it is known that the cold deciduous plants in Harvard Forest do not experience
10 water stress, no root water stress ($\beta = 1$ in Eq. 8) is assumed for additional simulations (LSM-
11 dvegNS and LSM-ovegNS). With the prescribed water stress factor of 1, the model captured
12 the observed NEP reasonably and overestimated GPP and RE compared to observations,
13 similar to MMSF simulations.

14 The ET in both LSM simulations were overestimated compared to the flux tower observations
15 in MMSF and Harvard Forest. These discrepancies might be attributed to both model and data
16 errors. In the model, the higher estimated GPP (although we cannot confirm this) may lead to
17 the overestimated ET to some extent, since higher photosynthesis corresponds to higher
18 canopy conductance and hence more transpiration. In addition, it is well known that eddy
19 flux measurements do not close the energy balance (Wilson et al. 2002). The sum of latent,
20 sensible and ground heat is generally smaller than the net shortwave radiation, which is often
21 caused by measurement errors of latent heat (i.e., ET) and sensible heat (Aranibar et al. 2006),
22 leading to imbalance in measured net radiation of as much as 20%. The LSM simulated peak
23 ET is within approximately 70% of measurements.

24 **4.2 Drought deciduous herbaceous plants**

25 **4.2.1 Phenology**

26 We evaluated the model performance for drought deciduous herbaceous and woody plants at
27 two sites, the Vaira Ranch and Tonzi Ranch in California. As shown in Fig. 6, at both sites,
28 the timings of C3 annual grasses' green-up and senescence are mainly controlled by soil
29 moisture in a Mediterranean climate, in which precipitation and temperature are seasonally
30 out of phase. Grasses are active during the winter rains, but slightly cold limited in activity,

1 then with spring warming, growth and activity increase, followed by rapid senescence that
2 closely tracks soil moisture dry-down in the late spring, and full senescence by the beginning
3 of the dry, hot summer. At the Tonzi Ranch, the oaks have the opposite seasonality to the C3
4 grasses. The oaks leaf out at the end of winter rains around March, when grasses have
5 reached their peak, and then the trees start gradually losing their leaves around the beginning
6 of July due to drought stress. Their complete leaf-off appears to be cued by November cold or
7 fog, but this latter cue would not be considered a stress factor and is not well understood.

8 At both Vaira and Tonzi Ranches, Ent-dveg and LSM-dveg reasonably captured these
9 phenological timings (Fig. 6). The growth rate for herbaceous plants (i.e., increase in LAI
10 during the growing season) reflected the net carbon assimilation each day, and slightly lagged
11 observations at the beginning of the growing season in the model. Simulated soil moisture
12 clearly decreased much more slowly in LSM-dveg during the late spring dry-down compared
13 to the observed volumetric soil moisture that was used to drive Ent-dveg.

14 **4.2.2 Fluxes**

15 For carbon fluxes at the Vaira Ranch, the model simulations generally followed the observed
16 seasonality, although the late leaf-off in LSM-dveg leads to overestimation of carbon uptake
17 significantly, and the observed abrupt increase in R_E in the beginning of the growing season
18 was not captured in all cases (Fig. 7 and Table 6). Xu and Baldocchi (2004) suggest that the
19 large pulse of R_E is the consequence of quickly stimulated microbial activity in decomposition
20 after rain events during the dry season. In the Ent TBM, the soil moisture dependency of
21 decomposition is parameterized as a linear function of soil saturation percent (S) with a
22 plateau when $S > S_{opt}$ (70%). This response is derived from raw data of soil respiration
23 responses to temperature and moisture in grassland and winter wheat soils from Del Grosso et
24 al. (2005). Most likely, the damped response is because the Ent TBM does not model a
25 separate litter layer on top of the soil, and litter quality may not be well parameterized to
26 allow for fast turnover. As this is a soil model issue, further analysis is worthy of a separate
27 study.

28 At the Tonzi Ranch, the simulated NEP resulted in an RMSE of $\sim 0.4 \mu\text{mol/m}^2/\text{s}$ compared to
29 the observed flux (Fig. 7 and Table 6). During the late spring soil moisture dry-down period,
30 the grasses senesced and the oaks retained their leaves. The oaks started reducing their
31 carbon assimilation due to water stress, as the Ball-Berry slope (m; slope for stomatal

1 conductance) is scaled linearly with the water stress in the model. In reality, the oaks at Tonzi
2 adjust their osmotic potential to maintain their water potential, so their leaf water potential is
3 not linear with soil moisture (Kiang 2002). Therefore even with the reasonable LAIs in Ent-
4 oveg, Ent-dveg and LSM-dveg, the underestimated NEP and GPP in the summer are to be
5 expected, lacking a non-linear response function. Meanwhile, the overestimated LAI in
6 LSM-dveg clearly led to overestimated NEP and GPP. Furthermore, we found the soil
7 biogeochemistry model did not capture the soil respiration pulses after the rainfall, as in
8 Vaira.

9 The model reasonably captured the observed seasonality of ET with an R of ~ 0.9 in Vaira
10 and ~ 0.8 in Tonzi, while the R values for carbon fluxes were much lower. The water fluxes
11 were not much different between LSM-dveg vs. LSM-oveg, while the carbon fluxes were
12 significantly different due to different LAIs between the two. The differences in transpiration,
13 resulting from different LAIs, were compensated by evaporation, leading to a relative small
14 discrepancy in ET between the two experiments. Furthermore, the amplitudes (difference
15 between the maximum and the minimum) of ET were clearly damped in the model, with
16 underestimated peak fluxes during the growing season and overestimated fluxes during the
17 non-growing season. In particular, the noticeable amount of ET occurred during the non-
18 growing season in Vaira, suggesting the partitioning of ET into evaporation and transpiration
19 should be further investigated.

20 **4.3 Frost-hardening in evergreen cold-climate plants**

21 **4.3.1 Phenology**

22 At Hyytiala, the phenological behavior of interest is frost-hardening, which lowers
23 photosynthetic capacity in the winter. In comparison to observed LAI, assumed according to
24 Kolari (personal communication, 2007) as explained in Section 3.2. simulated LAIs (Ent-dveg
25 and LSM-dveg) (Fig. 8) were almost constant at $4 \text{ m}^2/\text{m}^2$ throughout the year, without much
26 decrease during the winter. For evergreen plants, LAI variations in the model reflect the
27 change in foliage carbon balance, as the phenological factor for evergreens remains 1 all the
28 time. Thus, the relatively constant LAIs mean no significant carbon losses during the winter
29 in the model. Based on additional Ent-dveg and LSM-dveg without frost-hardening (not
30 shown), we found that such discrepancy in LAI between observation and simulation itself did
31 not influence the predicted water and carbon fluxes noticeably.

1 **4.3.2 Fluxes**

2 Modeled frost-hardening in the spring improved the predicted seasonality of NEP markedly in
3 both Ent and LSM simulations (Fig. 8 and Table 6). Frost-hardening suppressed
4 photosynthetic capacity during the winter (particularly in Feb-April) and therefore GPP and
5 NEP. It also suppressed transpiration and thus ET, but a relatively small difference in ET was
6 detected between the simulations with and without the frost-hardening scheme as the RMSEs
7 with observations were 7.88 mm/s and 7.89 mm/s, respectively (Table 6).

8 With regard to the differences between the Ent-standalone and Ent-LSM models (Ent-dveg
9 vs. LSM-dveg), we found the magnitude of NEP was overestimated in Ent-dveg due to high
10 simulated GPP and underestimated in LSM-dveg due to low soil moisture. During the
11 growing season, the observed volumetric soil moisture was above $\sim 0.35 \text{ m}^3/\text{m}^3$, and the
12 resulting root water stress factor was 1 (completely unstressed) most of the time in Ent-dveg
13 (driven with the observed soil moisture and temperature). However, the predicted volumetric
14 soil moisture was below $\sim 0.25 \text{ m}^3/\text{m}^3$ during the growing season in the top 3 soil layers and
15 the plants roots experienced an average water stress factor of 0.68. Such underestimated soil
16 moisture in the Ent-LSM led to low estimates of NEP.

17

18 **5 Discussion**

19 Our experiments show that phenological timing of leaf-out and senescence can be fairly well
20 captured within 10 days or better of observations for deciduous or annual vegetation when
21 based on cumulative weather statistics (air and soil temperature, growing degree days, day
22 length) derived from observations in the literature. However, the response to soil moisture is
23 sensitive to whether deep root water access is represented to offset soil moisture stress in
24 shallower soil. Also the soil moisture response must be tuned to the given measure or land
25 model, because soil water content as simulated at the spatial resolution of a land surface
26 hydrology model does not correspond well with any field measure of soil moisture (e.g.
27 volumetric water content, matric potential, pre-dawn water potentials). Stomatal conductance
28 and soil respiration are sensitive to soil moisture stress and hence subject to inaccuracy
29 dependent on the soil moisture representation. Meanwhile, we uncovered weaknesses in the
30 representation of particular vegetation processes – autotrophic respiration and ED-based

1 carbon allocation – that, besides differences in simulated LAI at one site, were the primary
2 causes of differences from observed NEP.

3 **5.1 Drought deciduousness**

4 In Vaira grassland and Tonzi savanna, the phenology parameters, which are based on the
5 plant water stress factor (a function of soil moisture), were derived from the site observations
6 of volumetric soil water content (Eq. 8), and they perform well with observed soil moisture in
7 Ent but not with simulated soil moisture in the LSM. The GISS LSM model predicted the
8 same seasonal trends of soil moisture but higher in magnitude and lower in variability than
9 observations. Koster et al. (2009) point out that simulated soil moisture is a model-specific
10 quantity and thus that can be considered as an “index” of the moisture state. The specific
11 evaporation and runoff formulations, in addition to model-specific soil parameters such as
12 porosity, hydraulic conductivity, wilting point and layer depth defines a dynamic range of soil
13 moisture simulated by the certain model. Therefore the true information content of soil
14 moisture data lies not necessarily in their absolute magnitudes but in their time variability.

15 Therefore, the current approach using the absolute soil moisture value for water-limited
16 phenology parameterization could be improved by properly mapping the soil moisture values
17 from the field sites into those in the model, or by using the surrogates for the soil moisture,
18 such as VPD as suggested by Jolly et al. (2005). However, Stöckli et al. (2011) note that
19 VPD may not be a good indicator of deep soil moisture.

20 For the trees at MMSF and Harvard Forest, LSM-simulated water stress where the plants
21 should be unstressed indicates that calculating the water stress factor by weighting by root
22 depth distributions does not accurately reflect how trees actually access water. Deep roots
23 generally supply water when shallow layers are dry, and many trees perform hydraulic lift. A
24 future revision of the Ent water stress scheme will account for the ability of plants
25 preferentially to access soil moisture at any depth in the root zone, such that soil moisture
26 stress is not a simple weighted average through the root profile.

27 While the Fluxnet data have been widely used to evaluate the DGVMs and LSMs recently, we
28 still found the need for more comprehensive measurements at the sites. Specifically, it was
29 very difficult to have continuous soil moisture and temperature together along with
30 measurements with eddy covariance towers; also the detailed tree surveys were not always
31 available.

1 **5.2 Cold deciduousness**

2 For cold deciduous trees, we used the growing degree days and chilling requirements in
3 spring phenology (Botta et al., 2000) and temperature and photoperiod in fall phenology
4 (White et al., 1997; Jolly et al., 2005). While we have taken a widely used approach, some
5 recent studies suggest other possible approaches. For spring phenology, the importance of
6 photoperiod has been pointed out in recent studies (e.g., Korner and Basler, 2010;
7 Migliavacca et al., 2012). Korner and Basler (2010) suggested that when the chilling
8 requirement is fulfilled, plants become receptive to photoperiod signals and such sensitivity to
9 photoperiod is found in late successional species in mature forests. For fall phenology,
10 Delpierre et al. (2009) used chilling degree day-photoperiod to model leaf coloring change for
11 deciduous trees in France, and Yang et al. (2012) and Archetti (2013) found the model
12 suitable for New England, US, with different parameter fits. In general, despite agreement
13 about overall climate cues for cold deciduousness, further work is needed to uncover site-
14 independent parameterizations.

15 **5.3 Photosynthesis and respiration parameters**

16 In this study, site-specific parameters were used according to the data availability. As in
17 Appendix D, some of parameters are generic for PFTs and some are site-specific. For the
18 model to be utilized at the global scale, further exploration is required to determine
19 geographic variation in and possible climatology-based prediction of parameters. Model
20 parameters for biophysics or ecosystem models have been inferred with various mathematical
21 techniques, such as a Monte Carlo simulation (Kleidon and Mooney 2000), data assimilation
22 with Kalman filtering (Mo et al. 2008, Stöckli et al. 2008), optimization with the Marquardt-
23 Levenberg method (Wang et al. 2007) and optimization with Simulated Annealing method
24 (Medvigy et al. 2009, Kim et al. 2012).

25 In general, vegetation biophysics models can replicate observed canopy fluxes of CO₂ well
26 when the vegetation structure is well-specified, but the same net flux can be predicted from
27 different levels of gross assimilation versus respiration. The main biophysical parameters
28 common to most models are the maximum leaf photosynthetic carboxylation rate, V_{cmax};
29 autotrophic respiration as a function of biomass, temperature, and activity; and leaf litter
30 quality, such as lignin content, for soil respiration. While V_{cmax} may be precisely measured
31 for a leaf, its value can be highly variable within a plant and seasonally. Currently in the Ent

1 model, V_{cmax} is only variably with PFT and temperature, and the intrinsic quantum
2 efficiency for J_{max} is constant. The seasonal variation of V_{cmax} , J_{max} , and SLA could be
3 introduced, pending better mechanistic understanding. A simple approach based on
4 photoperiod such as in Bauerle et al. (2012) would be possible.

5 Autotrophic respiration can range ~30-80% of annual GPP for different plant types (Falge et
6 al. 2002). These parameters, however, may not extrapolate to the global scale, and thus future
7 study is necessary to investigate global variation in parameterizations. In general, respiration
8 is poorly understood and cannot be modeled fully mechanistically, but must rely on bulk
9 parameterizations that effectively integrate numerous processes. Researchers have attempted
10 various approaches to grouping some respiratory fluxes (Amthor 2000, Cannell and Thornley
11 2000) as responsive to different drivers, though there is as yet no generally accepted scheme.
12 In Ent, the streams are maintenance respiration that is a function of biomass and responsive to
13 temperature, “light growth respiration” from photosynthetic activity, and “biosynthesis
14 respiration” from growth or turnover of plant tissues.

15 In Ent, using site-specific parameters for leaf photosynthetic capacity, V_{cmax} , constant
16 throughout the canopy, we observed a tendency toward higher GPP and higher ecosystem
17 respiration, R_E , compared to that inferred from tower observations when night-time
18 respiration temperature response is used to estimate R_E . These extremes in the two
19 components of the net flux are not necessarily unreasonable, since the Fluxnet respiration
20 product could be underestimated. The R_E data products we used were modeled, as typical,
21 with an exponential equation to fit the measured night-time CO_2 flux as a function of soil
22 temperature (Schmid et al. 2000). Such an estimate excludes daytime root respiration, which
23 increases with photosynthetic activity (Tang and Baldocchi 2005, Tang et al. 2005). With
24 regard to GPP, recent oxygen isotope work suggests that global gross primary productivity is
25 higher than traditional estimates (Welp et al. 2011). It is a well-known problem in ecosystem
26 science that GPP and respiration cannot be directly partitioned through current measurement
27 methods for net ecosystem exchange, although there are hopes for a solution now possibly
28 with measurements of solar-induced fluorescence (van der Tol et al. 2014).

29 **5.4 Carbon allocation/growth scheme**

30 We encountered deficiencies in the carbon allocation/growth scheme that we adopted from
31 the ED model. Although the current carbon allocation and growth scheme results in LAI that

1 is reasonable, with some phenological timing issues as noted, the maximum LAI is achieved
2 thanks to a cap on LAI by allometric relations to stem structure and plant density, while the
3 rest of the plant carbon balance is not realistic, particularly with regard to rate of LAI growth,
4 amount of seasonal sapwood growth and conversion to heartwood, accumulation of carbon
5 reserves, and allocation to reproduction. The on/off cues of the Ent phenological factor for
6 cold deciduous trees results in unrealistic fast full leaf-out, which could be rectified by
7 introduction of a physically-based cell growth elongation factor (Lockhart 1965). We also
8 found it would be more realistic to make carbon allocation to each live pool independent. The
9 ED scheme's allocation to one live biomass total and then partitioning among the live pools
10 can lead to unrealistic behaviors for sapwood patterns during spring growth and fall
11 senescence, due to a partitioning scheme for live carbon that does not account for the different
12 seasonal behaviors of each live pool. Finally, reproduction in ED currently is a fixed fraction
13 of assimilated carbon, which is problematic in the plant's overall carbon balance as a large
14 sink. Recent studies show that reproduction relies heavily on stored carbon, which often
15 accumulates over more than a year, such that growth of other plant tissue is never carbon
16 limited while large stores are kept in reserve. The ED scheme relies on the plant using nearly
17 all stored carbon for deciduous plants each year. Introducing reproductive allocation based on
18 thresholds proposed by Sala et al. (2012) would help rectify Ent's simulated plant carbon
19 balances such that trees are not always reaching the limit of carbon starvation. Besides
20 respiration, plant carbon allocation is currently still poorly understood. However, recent
21 studies with carbon tracers (Epron et al. 2012, Epron et al. 2012) are yielding new insights
22 that could be used to improve growth schemes that continue to be a weakness in dynamic
23 global vegetation models.

24

25 **6 Conclusions**

26 In this study, we evaluated the Ent TBM focusing on the seasonal dynamics of vegetation leaf
27 as well as carbon and water fluxes. In particular, we took a process-based approach,
28 evaluating the Ent-standalone model with observed LAI and Ent's prognostic active growth
29 submodel with observed soil moisture as well as coupled to the LSM model for prognostic
30 soil moisture, allowing us to identify parameterizations that need to be improved. For
31 herbaceous PFTs whose phenological timings depend on soil water availability, it is
32 inevitable to find errors in phenological timing in Ent-LSM simulations due to the

1 discrepancy in simulated soil moisture in the LSM. Also the predicted LAI of herbaceous
2 PFTs in Ent directly reflects the amount of assimilated carbon on the day and vice versa as
3 herbaceous PFTs allocate assimilated carbon only to active compartments (as they have no
4 structural tissue), and thus any errors in phenological timings propagate into errors in
5 biophysical processes. For tree PFTs, the Ent soil moisture stress scheme should be
6 improved to allow deep soil moisture access to override stress that might result from
7 weighting shallower dry soil layers too strongly.

8 This study evaluated the phenology and resulting seasonality of fluxes in the limited number
9 of sites, including 4 different PFTs. The Ent PFTs not tested in this study include deciduous
10 needleleaf plants, evergreen broadleaf plants, shrubs, arctic grasses and crops. Future work
11 will involve determining the efficacy of these PFT parameterizations at the global scale, and
12 the possibility of developing some of these parameters as functions of local climate as
13 obtained from either reanalysis data or from GCM climatology. In addition, we have
14 identified deficiencies in the carbon allocation scheme from the ED model that can be
15 rectified in future revision of Ent's growth submodel.

16 Future work will include development of phenology and allometry parameter sets that
17 are robust at the global scale, and soil moisture stress accounting for deeper soil access. In
18 addition, due to how ED allocates biomass to all live pools (foliage, sapwood, fine roots)
19 combined rather than allowing for separate dynamics, alternative carbon allocation schemes
20 that partition the dynamics of the live tissues must be developed for realistic plant carbon
21 balances.

22 This work sets the foundations for coupled land carbon-GCM simulations that can
23 utilize height-structured canopy data from remotely sensed lidar, to reduce uncertainty in
24 predictions of the land carbon balance through tighter links between seasonal growth
25 dynamics geometrical and biomass allometry of vegetation canopies. Because use of the
26 model at the global scale will involve community users who will continue to identify
27 parameter sets applicable for more climatically diverse distributions of the Ent TBM's plant
28 functional types, this paper is also written to serve as a detailed reference for these users for
29 appropriate interpretation of model results and parameter adjustment.

30

31 **Appendix A: Root profiles**

1 Depth profiles of root density are modifications of those in (Rosenzweig and
2 Abramopoulos 1997), revised to fit the PFT categorizations in the Ent TBM. These are
3 modeled as cumulative normalized root density distributions $F(z)$ of a PFT as:

$$4 \quad F(z) = a_{PFT} Z^{b_{PET}} \quad (A1)$$

5 where z is soil depth (m), and a and b are PFT-specific parameters, summarized in Table A1.
6 The cumulative distributions are plotted in Since soil layers in the NASA GISS land surface
7 model only are defined down to 3.5 m depth, maximum root depths are limited to this value.

9 **Appendix B. Soil biogeochemistry in the Ent Terrestrial Biosphere Model**

10 The soil biogeochemistry submodel of Ent is utilizes a slightly modified version of the
11 CASA' biosphere submodel originally implemented in the NCAR LSM and CSM 1.4 (Bonan,
12 1996; Randerson et al., 1997; Fung et al., 2005; Doney et al., 2006), which itself is a modified
13 version of the original NASA-CASA biosphere model (Potter et al., 1993). The soil model
14 determines terrestrial soil carbon pools and CO₂ fluxes from microbial respiration.

15 **B.1. CASA structure**

16 The soil biogeochemistry model consists of 3 litter C and N pools and 9 soil C and N
17 pools, as in CASA'. The pools currently are only simulated for the top 30 cm soil depth. This
18 layer accounts for nearly all observable soil respiration fluxes to the atmosphere, but not for full
19 long-term carbon stocks in deeper soil. Down to 100 cm and deeper would allow comparison to
20 existing global datasets of soil carbon and root depths (Batjes, et al., 1996ab; Jackson, et al.
21 1996). Appendix Figure B1 shows these 12 pools. Ent has an optional 30-100 cm deeper soil
22 layer that is not run in the current paper.

23 The various pools currently have fixed C:N ratios and turnover times, listed in Table B1. The
24 pools gain carbon and nitrogen from transfers from other pools, and losses to respiration and
25 transfers to other pools. These transfer and respiration fractions are listed in Table B2.

26 Soil micrometeorological conditions for the soil layers must be extrapolated from the soil
27 layering scheme of the land surface model. For example the GISS land surface hydrology has a
28 6-layer soil scheme with geometrically increasing layer thicknesses with depth (Rosenzweig &

1 Abramopoulus, 1997), so soil temperature and moisture for the soil biogeochemistry layers are
2 calculated through a weighted sum for the upper 30 cm.

3 In addition to the transfer coefficients in Table B2, three other rate coefficients are
4 used (following Randerson et al., 1997):

5 $fact_soilmic = 1.25;$

6 $fact_slow = 1.5;$

7 $fact_passive = 1.5.$

8 These are simply decomposition rate adjustment factors for soil microbial, slow, and passive
9 pools (respectively) *for crops only*; their values for all other PFTs is 1.

10 **B.2. Soil module interface with vegetation**

11 Physical inputs to the soil module from the land surface hydrology are volumetric soil
12 moisture, soil temperature, and soil texture (percentage of clay, sand, and silt). Biological
13 inputs consist of leaf, root, and wood litter (Figure B1). Model outputs are soil C (and N, not
14 used) pools and soil CO₂ flux. Ent calculates litterfall carbon from the leaf area times the
15 specific leaf area,

16 The relevant plant functional type (PFT)-dependent litter parameters (leaf, fine root,
17 and wood turnover times, litter C:N ratios, specific leaf area, and lignin contents) from Ent are
18 listed in Table B2. In addition to these parameters, a parameter representing the inverse of the
19 residence times of the litter pools, denoted $annk_{lit}$ (in units of yr^{-1}), was calculated as the
20 inverse of $lrage$ for leaf and root litter or of $woodage$ for wood litter (Potter et al., 1993).

21 **B.3. Temperature and moisture responses of soil respiration**

22 We replaced the CASA' temperature and soil moisture responses of soil respiration with new
23 functions derived from new fits to field data collected by Del Grosso et al. (2005). The Ent
24 TBM temperature response of soil respiration is a simple piece-wise linear model that
25 increases up to 30 °C, then flattens. In reality, the response to temperature is exponential up
26 to a certain optimum then declines, but a linear representation was chosen because it reduces
27 the computational time compared to that required for calling an exponential function, and
28 tests on field data show adequate performance for the purpose of predicting respiration fluxes
29 and soil carbon pools (unpublished). At high soil temperatures, soil moisture stress usually

1 occurs also, but because no measurement data were available for respiration at temperatures
 2 above 30 °C, the Ent model response does not represent a decline in soil respiration at high
 3 temperature. The linear temperature response of soil respiration is:

$$\text{linear } f_{\text{temperature}} = \begin{cases} \text{Intercept} = 0.04607913, T_{\text{soil}} \leq 0^{\circ}\text{C} & 5 \\ \frac{(1 - \text{Intercept})}{(30 - 0)} T_{\text{soil}} + \text{Intercept}, 0 < T_{\text{soil}} \leq 30^{\circ}\text{C} & 7 \\ 1, T_{\text{soil}} \geq 30^{\circ}\text{C} & 8 \end{cases} \quad (\text{B1})$$

9 More realistically, the temperature response is in nature an exponential response, so if there
 10 are no computational constraints, the following Q10 function as formulated in the original
 11 CASA' should be used:

$$\text{exponential } f_{\text{temperature}} = \text{Q10}^{\frac{T_{\text{soil,C}} - 30.0}{10.0}} \quad (\text{B2})$$

13 where Q10 has a typical value of 2.0.

14 The Ent TBM moisture response of soil respiration is similarly a piece-wise linear
 15 model that rises from 0 at zero soil moisture to 1.0 at a relative extractable water content
 16 (REW) of 0.7, where REW is the fraction of saturation above the hygroscopic point. Because
 17 there are no good functions for calculating hygroscopic point based on soil texture, we
 18 estimate the hygroscopic point as half of the wilting point. We note that it would be more
 19 precise to model the soil moisture response as an optimality curve, that rises from the soil
 20 hygroscopic point (minimum $T_{\text{soil,C}}$ for microbes) rather than wilting point (for plants) to some
 21 optimum, then declines as pore space becomes saturated and obstructs the flux of gases.
 22 However, lack of good algorithms to calculate the soil hygroscopic point for different soil
 23 textures necessitate this version of Ent relying on the wilting point as the point of minimum
 24 available soil moisture. We may later introduce a simple linear decline of the soil moisture
 25 response with saturation, but at present we have no data on the response to saturated
 26 conditions.

$$f_{\text{moisture}} = \begin{cases} 0, & \text{REW} \leq 0 & 27 \\ \frac{1}{0.7} \text{REW}, & 0 < \text{REW} \leq 0.7 & 28 \\ 1, & \text{REW} \geq 0.7 & 29 \end{cases} \quad (\text{B3})$$

1
2
3
4
5
6
7
8
9
10
11
12
13
14
15
16
17
18
19
20
21
22
23
24
25
26
27
28
29
30
31
32

The linear soil respiration temperature and moisture response functions are plotted in Appendix Figures B1 and B2, along with the original CASA' responses, and those of Del Grosso et al. (2005), whose data were re-analyzed to generate the Ent response functions.

Appendix C: Allocation

The labile carbon reserves in Ent are allocated into different plant biomass pools, including foliage, sapwood, heartwood, fine root and coarse root. In addition, turnover of tissue due to background litter fluxes is replenished from the carbon reserve pool. In nature, plants may allocate biomass to different compartments in response to many different controlling factors, such as light availability and water availability, which alter, for example, root:shoot ratios. Among various carbon allocation modeling approaches with different complexities, many DGVMs take a simple approach to model carbon allocation via empirical and allometric relationships, a traditional 'static allocation' approach (Foley et al. 1996, Sitch et al. 2003) while some models parameterize the dependency of carbon allocation on resource availability, 'dynamic allocation' approach (Friedlingstein et al. 1999, Arora and Boer 2005). Although carbon allocation varies with plant status such as size and age, and environmental conditions, the static allocation approach may be justified for models operating at the large scale. If plant productivity is assumed in a steady state, carbon allocation is likely to be in a steady state. Also, spatial variability in environmental factors and their effects on allocation can be averaged. However, the fixed allocation approach is limited in long-term simulations as it lacks response to environmental changes such as climate change and elevated atmospheric CO₂ (Franklin et al. 2012). However, recent models of 'dynamic allocation' have been difficult to constrain due to a dearth of observations.

In the Ent TBM, the allocation submodel takes a traditional approach of 'static allocation', based on allometric relationships between different pools. Modified from approaches of the ED models (Moorcroft et al. 2001, Medvigy et al. 2009), the scheme allocates the labile carbon to different biomass pools according to empirical allometric relationships and leaf phenological status on a daily basis.

C.1. Active biomass

1 The biomass within each plant is partitioned between an active carbon pool and a structural
 2 carbon pool. The active biomass pool (B_{active}) ($\text{kg}_{\text{biomass}}/\text{cohort}$) is sub-divided into foliage
 3 (B_{fol}), sapwood (B_{sw}) and fine roots (B_{froot}) which turn over at different rates, while the
 4 structural pool ($B_{structural}$) consists of heartwood (B_{hw}) and coarse roots (B_{croot}). Grasses do not
 5 have the structural pool. The labile biomass (B_{lab}) assimilated on the same day is allocated to
 6 the active carbon pool to maintain the size of foliage, sapwood and fine root tissues given
 7 their turnover rates, and to accumulate the active carbon up to its maximum.

8 Thus, the time change of the active pool can be written by

$$9 \quad \frac{dB_{active}}{dt} = \min [\min(B_{lab}, CB_d), B_{active}^{max} - B_{active}] \quad (C1)$$

10 where B_{active}^{max} is the maximum active carbon of each plant, which is determined according to
 11 the maximum foliage carbon according to the size of plant, CB_d is the daily plant carbon
 12 balance (i.e., sum of NPP on one day). Then, the allometric relationships are used to sub-
 13 divide the active biomass into its components. The foliage biomass is determined according
 14 to its phenological status (φ), ranging from 0 (for full senescence) to 1 (full leaf-out), as a
 15 proportion of full-leaved foliage biomass, B_{fol}^* , so that $B_{fol} = \varphi B_{fol}^*$. Both the fine root and
 16 sapwood biomass are also determined according to their proportional relationships to B_{fol}^* . A
 17 constant empirical proportionality for fine root (q_{fr}), assumed to be 1, is related as:

$$18 \quad q_{fr} = \frac{B_{froot}}{B_{fol}^*} = 1 \quad (C2)$$

19 The sapwood biomass is determined according to the pipe-model theory (Shinozaki et al.
 20 1964), which suggests that the total foliage area is proportional to the sapwood cross-sectional
 21 area. The ratio between full-leaved foliage area and sapwood area is assumed to be 3900
 22 ($\text{m}^2_{\text{foliage}}/\text{m}^2_{\text{sapwood}}$). This value is adopted from the value used in ED1 (Moorcroft et al. 2001),
 23 which follows Rending and Taylor (1989), giving the ratios of foliage area to sapwood area
 24 ranging from 3900 to 14000. These assumptions result in the following relationship:

$$25 \quad \frac{(\text{foliage area})}{(\text{sapwood area})} = \frac{SLA \cdot B_{fol}^*}{\frac{B_{sw}}{\rho_{sw} \cdot h}} = 3900 \quad (C3)$$

26 where ρ_{sw} is the sapwood density ($\text{kgC}/\text{m}^3_{\text{sapwood}}$) and SLA is the specific leaf area
 27 ($\text{m}^2_{\text{foliage}}/\text{kgC}$) for each PFT, provided in Table 1. ρ_{sw} is taken to be 500 ($\text{kgC}/\text{m}^3_{\text{sapwood}}$) (i.e.,
 28 $0.5 \text{kgC}/\text{kg}_{\text{biomass}} \times 1000 \text{kg}_{\text{biomass}}/\text{m}^3_{\text{sapwood}}$ for very hard wood). However, we note that there
 29 are departures from these constant values. The fraction of dry biomass that is carbon in

1 spruce wood is typically 0.48 (Payne 2002). Also, Schneider et al. (2011) find the foliage to
 2 sapwood area ratio to be closer to 500-600 for Jack pine, with higher values toward the
 3 interior of the sapwood that serves older foliage. Calvo-Alvarado et al. (2008) find an
 4 increasing linear relation between height and foliage area/sapwood area for Costa Rican
 5 rainforest trees, ranging from 500-1500. A consistent rule for this variation has yet to be
 6 identified, but it may vary with wood density and anatomy.

7 Finally, B_{fol} is related to LAI ($m^2_{foliage}/m^2_{ground}$), measuring the total leaf (i.e., foliage) area per
 8 the projected ground area by

$$9 \quad LAI = 0.5 \cdot B_{fol} \cdot SLA \cdot n_{plant} \quad (C4)$$

10 where n_{plant} is the population density of cohorts (# plants/ m^2_{ground}), and 0.5 ($kgC/kg_{biomass}$) is
 11 to convert SLA in $m^2_{foliage}/kgC$ to $m^2_{foliage}/kg_{biomass}$.

12 **C.2. Structural and reproductive biomass**

13 Growth of structural tissue is handled as follows. If the stored labile biomass is non-zero, the
 14 size of the structural pool of woody plants increases according to the empirical allometric
 15 relationships and consequently the size of the active pool increases. Here, the partitioning
 16 between B_{active} and $B_{structural}$ is written by

$$17 \quad q_{structural} = \frac{dB_{structural}}{dB_{active}} = \frac{\frac{dDBH}{dB_{active}}}{\frac{dDBH}{dB_{structural}}} \quad (C5)$$

18 where DBH is the diameter at breast height and $q_{structural}$ is the ratio of structural growth to
 19 active growth. The derivatives are derived from allometric relationships according to plant
 20 size (i.e., DBH , and height) for woody plants. Note herbaceous plants do not have the
 21 structural pool, meaning that $DBH=0$, $q_{structural}=0$, $B_{structural}=0$, and $q_{sw}=0$. Also, the plant
 22 devotes a fixed fraction (q_{repro}) of daily carbon to the reproductive pool and the rest to growth
 23 of the active and structural pools. q_{repro} is assumed to be 0.3 for woody plants and 1.0 for
 24 herbaceous plants, following the assumptions of ED1 (Moorcroft et al. 2001).

1 **Appendix D: Biophysics, Allocation, and Phenology Parameters**

2 See Table D1 and D2.

3

4

6 **Code Availability**

7 The Ent TBM is being developed as a part of NASA GISS ModelE. Version 1.0.0.0, Ent
8 biophysics, is available in <http://data.giss.nasa.gov/modelE/> (Schmidt et al, 2014). As noted in
9 the main text, users of this version of Ent phenology and growth, version 1.0.1.0.0, are
10 encouraged to use it for site-based studies with parameters derived at the site level, not for
11 global studies. Since Ent TBM v1.0.1.0.0 does not yet apply at the global scale, it is not
12 released yet in ModelE for GCM use, but the code used in this study may be obtained by
13 contacting the corresponding author via email.

14

15 **Acknowledgements**

16 This research was supported by two grants from the NASA Earth Science, Modeling,
17 Analysis & Prediction Program (MAP/04-116-0069), for proposals titled ‘Ent: A Global
18 Dynamic Terrestrial Ecosystem Model for Climate Interactions at Seasonal to Century Time
19 Scales Through Coupled Water, Carbon, and Nitrogen Dynamics’ (PI: Nancy Y. Kiang), and
20 ‘NASA Goddard Institute for Space Studies Global Model Development’ (PI: James Hansen
21 and Gavin Schmidt). Support was also provided in part by an appointment of Yeonjoo Kim
22 to the NASA Postdoctoral Program at NASA GISS administered by Oak Ridge Associated
23 Universities through a contract with NASA, for a proposal titled ‘Role of phenology in
24 coupled vegetation-climate at seasonal to decadal timescales in Ent DGTEM’. We also wish
25 to express our gratitude to the many researchers who made available large amounts of data
26 from their Fluxnet sites, particularly Danilo Dragoni, HaPe Schmid, and Craig Wayson for
27 Morgan Monroe State Forest; Dennis Baldocchi for the Vaira and Tonzi Ranches; Steve
28 Wofsy and co-workers for Harvard Forest; and Timo Vesala and Pasi Kolari for Hyytiälä.
29 The websites of publicly available data are listed in Table 3.

30

31

1 **References**

- 2 Abramopoulos, F., Rosenzweig, C., and Choudhury, B. J.: Improved ground hydrology
3 calculations for global climate models (GCMs): soil water movement and evapotranspiration,
4 *J. Climate*, 1, 921–941, 1988.
- 5 Amthor, J. S.: The McCree–de Wit–Penning de Vries–Thornley respiration paradigms: 30
6 years later, *Ann. Bot.-London*, 86, 1–20, 2000.
- 7 Aranibar, J. N., Berry, J. A., Riley, W. J., Pataki, D. E., Law, B. E., and Ehleringer, J. R.:
8 Combining meteorology, eddy fluxes, isotope measurements, and modeling to understand
9 environmental controls of carbon isotope discrimination at the canopy scale, *Glob. Change*
10 *Biol.*, 12, 710–730, 2006.
- 11 Arora, V. K. and Boer, G. J.: A parameterization of leaf phenology for the terrestrial
12 ecosystem component of climate models, *Glob. Change Biol.*, 11, 39–59, 2005.
- 13 Badeck, F. W., Bondeau, A., Böttcher, K., Doktor, D., Lucht, W., Schaber, J., and Sitch, S.:
14 Responses of spring phenology to climate change, *New Phytol.*, 162, 295–309, 2004.
- 15 Baldocchi, D., Falge, E., Gu, L., Olson, R., Hollinger, D., Running, S., Anthoni, P.,
16 Bernhofer, C., Davis, K., Evans, R., Fuentes, J., Goldstein, A., Katul, G., Law, B., Lee, X.,
17 Malhi, Y., Meyers, T., Munger, W., Oechel, W., Paw U, K. T., Schmid, H. P., Valentini, R.,
18 Verma, S., Vesala, T., Wilson, K., and Wofsy, S.: FLUXNET: a new tool to study the
19 temporal and spatial variability of ecosystem-scale carbon dioxide, water vapor, and energy
20 flux densities, *B. Am. Meteorol. Soc.*, 82, 2415–2434, 2001.
- 21 Baldocchi, D., Xu, L. K., and Kiang, N.: How plant functional-type, weather, seasonal
22 drought, and soil physical properties alter water and energy fluxes of an oak-grass savanna
23 and an annual grassland, *Agr. Forest Meteorol.*, 123, 13–39, 2004.
- 24 Ball, J., Woodrow, L. E., and Beny, J. A.: A model predicting stomatal conductance and its
25 contribution to the control of photosynthesis under different environmental conditions, in:
26 *Progress in Photosynthesis research*, edited by: Biggins, J., Nijhoff, Dordrecht, 221–224,
27 1987.
- 28 Batalha, N. M., Rowe, J. F., Bryso, S. T. et al.: Planetary candidates observed by Kepler, III:
29 Analysis of the first 16 months of data, *The Astrophysical Journal Supplement Series*, 204, 24
30 (21 pp.), doi:10.1088/0067-0049/204/2/24, 2012.

- 1 Batjes, N. H.: Total carbon and nitrogen in the soils of the world, *European Journal of Soil*
2 *Science*, 47, 151-163, 1996.
- 3 Batjes, N. H.: Documentation to ISRIC-WISE global data set of derived soil properties on a
4 1/2 deg by 1/2 deg grid (Version 1.0), Wageningen, The Netherlands., International Soil
5 Reference and Information Centre (ISRIC), 1996.
- 6 Bonan, G. B.: A land surface model (LSM Version 1.0) for ecological, hydrological, and
7 atmospheric studies: technical description and user's guide, Boulder, Colorado, National
8 Center of Atmospheric Research, 122, 1996.
- 9 Bonan, G. B. and Levis, S.: Evaluating aspects of the community land and atmosphere models
10 (CLM3 and CAM3) using a Dynamic Global Vegetation Model, *J. Climate*, 19, 2290–2301,
11 2006.
- 12 Bonan, G. B., Levis, S., Sitch, S., Vertenstein, M., and Oleson, K. W.: A dynamic global
13 vegetation model for use with climate models: concepts and description of simulated
14 vegetation dynamics, *Glob. Change Biol.*, 9, 1543–1566, 2003.
- 15 Bonan, G. B., Lawrence, P. J., Oleson, K. W., Levis, S., Jung, M., Reichstein, M., Lawrence,
16 D. M. and Swenson, S. C.: Improving canopy processes in the Community Land Model
17 version 4 (CLM4) using global flux fields empirically inferred from FLUXNET data, *J.*
18 *Geophys. Res.- Biogeoe.*, 116, G02014, doi:10.1029/2010JG001593, 2011.
- 19 Botta, A., Viovy, N., Ciais, P., Friedlingstein, P., and Monfray, P.: A global prognostic
20 scheme of leaf onset using satellite data, *Glob. Change Biol.*, 6, 709–725, 2000.
- 21 Bradley, N. L., Leopold, A. C., Ross, J., and Huffaker, W.: Phenological changes reflect
22 climate change in Wisconsin, *P. Natl. Acad. Sci. USA*, 96, 9701–9704, 1999.
- 23 Calvo-Alvarado, J. C., McDowell, N. G., and Waring, R. H.: Allometric relationships
24 predicting foliar biomass and leaf area: sapwood area ratio from tree height in five Costa
25 Rican rain forest species, *Tree Physiol.*, 28, 1601–1608, 2008.
- 26 Cannell, M. G. R. and Thornley, J. H. M.: Modelling the components of plant respiration:
27 some guiding principles, *Ann. Bot.-London*, 85, 45–54, 2000.
- 28 Cox, P. M.: Description of the “TRIFFID” Dynamic Global Vegetation Model, London,
29 Hadley Centre, 16, 2001.

- 1 Cramer, W., Bondeau, A., Woodward, F. I., Prentice, I. C., Betts, R. A., Brovkin, V., Cox, P.
2 M., Fisher, V., Foley, J. A., Friend, A. D., Kucharik, C., Lomas, M. R., Ramankutty, N.,
3 Sitch, S., Smith, B., White, A., and Young-Molling, C.: Global response of terrestrial
4 ecosystem structure and function to CO₂ and climate change: results from six dynamic global
5 vegetation models, *Glob. Change Biol.*, 7, 357–373, 2001.
- 6 Defries, R. S., Field, C. B., Fung, I., Justice, C. O., Los, S. O., Matson, P. A., Matthews, E.,
7 Mooney, H. A., Potter, C., Prentice, K. C., Sellers, P. J., Townshend, J., Tucker, C. J., Ustin,
8 S. L., and Vitousek, P.: Mapping the land-surface for global atmosphere–biosphere models –
9 toward continuous distributions of vegetations functional-properites, *J. Geophys. Res.-*
10 *Atmos.*, 100, 20867–20882, 1995.
- 11 Del Grosso, S. J., Parton, W. J., Mosier, A. R., Holland, E. A., Pendall, E., Schimel, D. S.,
12 and Ojima, D. S.: Modeling soil CO₂ emissions from ecosystems, *Biogeochemistry*, 73, 71–
13 91, 2005.
- 14 Delire, C. and Foley, J. A.: Evaluating the performance of a land Surface/ecosystem model
15 with biophysical measurements from contrasting environments, *J. Geophys. Res.-Atmos.*,
16 104, 16895–16909, 1999.
- 17 Dickinson, R. E., Shaikh, M., Bryant, R., and Graumlich, L.: Interactive canopies for a
18 climate model, *Journal of Climate*, 11, 2823–2836, 1998.
- 19 Dirmeyer, P. A.: Vegetation stress as a feedback mechanism in midlatitude drought, *J.*
20 *Climate*, 7, 1463–1483, 1994.
- 21 Dragoni, D., Schmid, H. P., Grimmond, C. S. B., and Loescher, H. W.: Uncertainty of annual
22 net ecosystem productivity estimated using eddy covariance flux measurements, *J. Geophys.*
23 *Res.-Atmos.*, 112, D17102, doi:10.1029/2006JD008149, 2007.
- 24 Dunne, J. P., John, J. G., Shevliakova, E., Stouffer, R. J., Krasting, J. P., Malyshev, S. L.,
25 Milly, P. C. D., Sentman, L. T., Adcroft, A. J., Cooke, W., Dunne, K. A., Griffies, S. M.,
26 Hallberg, R. W., Harrison, M. J., Levy, H., Wittenberg, A. T., Phillips, P. J., and Zadeh, N.:
27 GFDL’s ESM2 Global Coupled Climate-Carbon Earth System Models. Part II: Carbon
28 System Formulation and Baseline Simulation Characteristics, *J. Climate*, 26, 2247–2267,
29 2013.
- 30 Epron, D., Bahn, M., Derrien, D., Lattanzi, F. A., Pumpanen, J., Gessler, A., Hogberg, P.,
31 Maillard, P., Dannoura, M., Gerant, D., and Buchmann, N.: Pulse-labelling trees to study

1 carbon allocation dynamics: a review of methods, current knowledge and future prospects,
2 *Tree Physiol.*, 32, 776–798, 2012a.

3 Epron, D., Laclau, J.-P., Almeida, J. C. R., Gon Balves, J. L. M., Ponton, S., Sette Jr., C. R.,
4 Delgado-Rojas, J. S., Bouillet, J.-P., and Nouvellon, A. Y.: Do changes in carbon allocation
5 account for the growth response to potassium and sodium applications in tropical Eucalyptus
6 plantations?, *Tree Physiol.*, 32, 667–679, 2012b.

7 Falge, E., Baldocchi, D., Tenhunen, J., Aubinet, M., Bakwin, P., Berbigier, P., Bernhofer, C.,
8 Burba, G., Clement, R., Davis, K. J., Elbers, J. A., Goldstein, A. H., Grelle, A., Granier, A.,
9 Guðmundsson, J., Hollinger, D., Kowalski, A. S., Katul, G., Law, B. E., Malhi, Y., Meyers,
10 T., Monson, R. K., Munger, J. W., Oechel, W., Paw U, K. T., Pilegaard, K., Rannik, Ü.,
11 Rebmann, C., Suyker, A., Valentini, R., Wilson, K., and Wofsy, S.: Seasonality of ecosystem
12 respiration and gross primary production as derived from FLUXNET measurements, *Agr.*
13 *Forest Meteorol.*, 113, 75–95, 2002.

14 Farquhar, G. and Von Caemmerer, S.: Modeling photosynthetic response to environmental
15 conditions, in: *Encyclopedia of Plant Physiol.*, edited by: Lange, O. L., Nobel, P. S., Os
16 mond, C. B., and Ziegler, H., Springer-Verlag, Berlin, 549–587, 1982.

17 Farquhar, G. D., Caemmerer, S. V., and Berry, J. A.: A biochemical model of photosynthetic
18 CO₂ assimilation in leaves of C₃ species, *Planta*, 149, 78–90, 1980.

19 Foley, J. A., Prentice, I. C., Ramankutty, N., Levis, S., Pollard, D., Sitch, S., and Haxeltine,
20 A.: An integrated biosphere model of land surface processes, terrestrial carbon balance, and
21 vegetation dynamics, *Global Biogeochem. Cy.*, 10, 603–628, 1996.

22 Franklin, O., Johansson, J., Dewar, R. C., Dieckmann, U., McMurtrie, R. E., Brannstrom, A.,
23 and Dybzinski, R.: Modeling carbon allocation in trees: a search for principles, *Tree Physiol.*,
24 32, 648–666, 2012.

25 Friedlingstein, P., Joel, G., Field, C. B., and Fung, I. Y.: Toward an allocation scheme for
26 global terrestrial carbon models, *Glob. Change Biol.*, 5, 755–770, 1999.

27 Friedlingstein, P., Cox, P., Betts, R., Bopp, L., Von Bloh, W., Brovkin, V., Cadule, P., Doney,
28 S., Eby, M., Fung, I., Bala, G., John, J., Jones, C., Joos, F., Kato, T., Kawamiya, M., Knorr,
29 W., Lindsay, K., Matthews, H. D., Raddatz, T., Rayner, P., Reick, C., Roeckner, E.,
30 Schnitzler, K.- G., Schnur, R., Strassmann, K., Weaver, A. J., Yoshikawa, C., and Zeng, N.:

- 1 Climate-carbon cycle feedback analysis: results from the C(4)MIP model intercomparison, J.
2 Climate, 19, 3337–3353, 2006.
- 3 Friedlingstein, P., Meinshausen, M., Arora, V. K., Jones, C. D., Anav, A., Liddicoat, S. K.,
4 and Knutti, R.: Uncertainties in CMIP5 climate projections due to carbon cycle feedbacks, J.
5 Climate, 27, 511–526, 2014.
- 6 Friend, A. D., Arneth, A., Kiang, N. Y., Lomas, M., Ogée, J., Rödenbeck, C., Running, S. W.,
7 Santaren, J.-D., Sitch, S., Viovy, N., Woodward, F. I., and Zaele, S.: FLUXNET and
8 modelling the global carbon cycle, Glob. Change Biol., 13, 610–633, 2007.
- 9 Fung, I., Doney, S., Lindsay, K., and John, J.: Evolution of carbon sinks in a changing
10 climate, Proc Natl Acad Sci, 102, 11201–11206, 2005.
- 11 Goulden, M. L., Munger, J. W., Fan, S. M., Daube, B. C., and Wofsy, S. C.: Exchange of
12 carbon dioxide by a deciduous forest: response to interannual climate variability, Science,
13 271, 1576–1578, 1996.
- 14 Hanninen, H. and Kramer, K.: A framework for modelling the annual cycle of trees in boreal
15 and temperate regions, Silva Fenn., 41, 167–205, 2007.
- 16 Hutrya, L. R., Munger, J. W., Saleska, S. R., Gottlieb, E., Daube, B. C., Dunn, A. L., Amaral,
17 D. F., de Camargo, P. B., and Wofsy, S. C.: Seasonal controls on the exchange of carbon and
18 water in an Amazonian rain forest, J. Geophys. Res.-Biogeo., 112, G03008,
19 doi:10.1029/2006JG000365, 2007.
- 20 Ilvesniemi, H. and Liu, C.: Biomass distribution in a young Scots pine stand, Boreal Environ.
21 Res., 6, 3–8, 2001.
- 22 Jackson, R. B., Canadell, J., Ehleringer, J. R., Mooney, H. A., Sala, A., and Schulze, E. D.: A
23 global analysis of root distributions for terrestrial biomes, Oecologia, 108, 389–411, 1996.
- 24 Jolly, W. M. and Running, S. W.: Effects of precipitation and soil water potential on drought
25 deciduous phenology in the Kalahari, Glob. Change Biol., 10, 303–308, 2004.
- 26 Jolly, W. M., Nemani, R., and Running, S. W.: A generalized, bioclimatic index to predict
27 foliar phenology in response to climate, Glob. Change Biol., 11, 619–632, 2005.
- 28 Keeling, C. D., Chin, J. F. S., and Whorf, T. P.: Increased activity of northern vegetation
29 inferred from atmospheric CO₂ measurements, Nature, 382, 146–149, 1996.

- 1 Kiang, N. Y.: Savannas and seasonal drought: the landscape-leaf connection through optimal
2 stomatal control, in: Environmental Science, Policy and Management, University of
3 California at Berkeley, Berkeley, 303 pp., 2002.
- 4 Kim, Y. and Wang, G. L.: Impact of vegetation feedback on the response of precipitation to
5 antecedent soil moisture anomalies over North America, *J. Hydrometeorol.*, 8, 534–550,
6 2007.
- 7 Kim, Y., Knox, R. G., Longo, M., Medvigy, D., Hutyrá, L. R., Pyle, E. H., Wofsy, S. C.,
8 Bras, R. L., and Moorcroft, P. R. Seasonal carbon dynamics and water fluxes in an Amazon
9 rainforest, *Glob. Change Biol.*, 18, 1322–1334, 2012.
- 10 Kleidon, A. and Mooney, H. A.: A global distribution of biodiversity inferred from climatic
11 constraints: results from a process-based modelling study, *Glob. Change Biol.*, 6, 507–523,
12 2000.
- 13 Koster, R. D., Guo, Z., Dirmeyer, P. A., Yang, R., Mitchell, K., and Puma, M. J.: On the
14 nature of soil moisture in land surface models, *J. Climate*, 22, 4322–4335, 2009.
- 15 Kramer, K., Leinonen, I., and Loustau, D.: The importance of phenology for the evaluation of
16 impact of climate change on growth of boreal, temperate and Mediterranean forests
17 ecosystems: an overview, *Int. J. Biometeorol.*, 44, 67–75, 2000.
- 18 Krinner, G., Viovy, N., de Noblet-Ducoudré, N., Ogée, J., Polcher, J., Friedlingstein, P.,
19 Ciais, P., Sitch, S., and Prentice, I. C.: A dynamic global vegetation model for studies of the
20 coupled atmosphere–biosphere system, *Global Biogeochem. Cy.*, 19, GB1015,
21 doi:10.1029/2003GB002199, 2005.
- 22 Kucharik, C., Barford, C., El Maayar, M., Wofsy, S. C., Monson, R. K., and Baldocchi, D. D.:
23 A multiyear evaluation of a Dynamic Global Vegetation Model at three AmeriFlux forest
24 sites: vegetation structure, phenology, soil temperature, and CO₂ and H₂O vapor exchange,
25 *Ecol. Model.*, 196, 1–31, 2006.
- 26 Levis, S. and Bonan, G. B.: Simulating springtime temperature patterns in the community
27 atmosphere model coupled to the community land model using prognostic leaf area, *J.*
28 *Climate*, 17, 4531–4540, 2004.
- 29 Lockhart, J. A.: An analysis of irreversible plant cell elongation, *J. Theor. Biol.*, 8, 264–275,
30 1965.

- 1 Makela, A., Hari, P., Berninger, F., Hanninen, H., and Nikinmaa, E.: Acclimation of
2 photosynthetic capacity in Scots pine to the annual cycle of temperature, *Tree Physiol.*, 24,
3 369–376, 2004.
- 4 Mäkelä, A., Kolari, P., Karimäki, J., Nikinmaa, E., Perämäki, M., and Hari, P.: Modelling five
5 years of weather-driven variation of GPP in a boreal forest, *Agr. Forest Meteorol.*, 139, 382–
6 398, 2006.
- 7 Matthews, E.: Global vegetation and land use: new high-resolution data bases for climate
8 studies, *Journal of Climate and Applied Meteorology*, 22, 474-487, 1983.
- 9 Medvigy, D., Walko, R. L., and Avissar, R.: Modeling interannual variability of the Amazon
10 hydroclimate, *Geophys. Res. Lett.*, 35, L15817, doi:10.1029/2008GL034941, 2008.
- 11 Medvigy, D., Wofsy, S. C., Munger, J. W., Hollinger, D. Y., and Moorcroft, P. R.:
12 Mechanistic scaling of ecosystem function and dynamics in space and time: ecosystem
13 demography model version 2, *J. Geophys. Res.*, 114, G01002, doi:10.1029/2008JG000812,
14 2009.
- 15 Menzel, A.: Trends in phenological phases in Europe between 1951 and 1996, *Int. J.*
16 *Biometeorol.*, 44, 76–81, 2000.
- 17 Mo, X., Chen, J. M., Ju, W., and Black, T. A.: Optimization of ecosystem model parameters
18 through assimilating eddy covariance flux data with an ensemble Kalman filter, *Ecol. Model.*,
19 217, 157–173, 2008.
- 20 Moorcroft, P. R., Hurtt, G. C., and Pacala, S. W.: A method for scaling vegetation dynamics:
21 the ecosystem demography model (ED), *Ecol. Monogr.*, 71, 557–585, 2001.
- 22 Ni-Meister, W., Yang, W. Z., and Kiang, N. Y.: A clumped-foliage canopy radiative transfer
23 model for a global dynamic terrestrial ecosystem model, I: Theory, *Agr. Forest Meteorol.*,
24 150, 881–894, 2010.
- 25 Payne, C.: Modification of the nitrogen content and C:N ratio of Sitka spruce timber by kiln
26 and air drying, de Gruyter, Berlin, Allemagne, 2002.
- 27 Potter, C. S., Randerson, J. T., Field, C. B., Matson, P. A., Vitousek, P. M., Mooney, H. A.,
28 and Klooster, S. A.: Terrestrial ecosystem production: a process model based on global
29 satellite and surface data, *Global Biogeochem. Cy.*, 7, 811–841, 1993.

1 Pumpanen, J., Heinonsalo, J., Rasilo, T., Villemot, J., and Ilvesniemi, H.: The effects of soil
2 and air temperature on CO₂ exchange and net biomass accumulation in Norway spruce, Scots
3 pine and silver birch seedlings, *Tree Physiol.*, 32, 724–736, 2012.

4 Randerson, J. T., Thompson, M. V., Conway, T. J., Fung, I. Y., and Field, C. B.: The
5 contribution of terrestrial sources and sinks to trends in the seasonal cycle of atmospheric
6 carbon dioxide, *Global Biogeochemical Cycles*, 11, 535-560, 1997.

7 Randerson, J. T., Hoffman, F. M., Thornton, P. E., Mahowald, N. M., Lindsay, K., Lee, Y. H.,
8 Nevison, C. D., Doney, S. C., Bonan, G., Stockli, R., Covey, C., Running, S. W., and Fung, I.
9 Y.: Systematic assessment of terrestrial biogeochemistry in coupled climate-carbon models,
10 *Glob. Change Biol.*, 15, 2462–2484, 2009.

11 Reich, P. B., Wright, I. J., and Lusk, C. H.: Predicting leaf physiology from simple plant and
12 climate attributes: a global GLOPNET analysis, *Ecol. Appl.*, 17, 1982–1988, 2007.

13 Repo, T., Makela, A., and Hanninen, H.: Modelling frost resistance of trees, in: *Modelling to*
14 *Understand Forest Function*, edited by: Jozefek, H., *Silva Carelica*, 61–74, 1990.

15 Richardson, A. D., Anderson, R. S., Arain, A. M., Barr, A. L. A. N. G., Bohrer, G., Chen, G.,
16 Chen, J. M., Ciais, P., Davis, K. J., Desai, A. R., Dietze, M. C., Dragoni, D., Garrity, S. R.,
17 Gough, C. M., Grant, R., Hollinger, D. Y., Margolis, H. A. N. K. A., McCaughey, H., Migli
18 avacca, M., Monson, R. K., Munger, W. J., Poulter, B., Raczka, B. M., Ricciuto, D. M.,
19 Sahoo, A. K., Schaefer, K. E. V. I. N., Tian, H., Vargas, R., Verbeeck, H., Xiao, J., and Xue,
20 Y.: Terrestrial biosphere models need better representation of vegetation phenology: results
21 from the North American Carbon Program Site Synthesis, *Glob. Change Biol.*, 18, 566–584,
22 2012.

23 Richardson, A. D., Keenan, T. F., Migliavacca, M., Ryu, Y., Sonnentag, O., and Toomey, M.:
24 Climate change, phenology, and phenological control of vegetation feedbacks to the climate
25 system, *Agr. Forest Meteorol.*, 169, 156–173, 2013.

26 Rodriguez-Iturbe, I., Porporato, A., Laio, F., and Ridolfi, L.: Plants in water-controlled
27 ecosystems: active role in hydrologic processes and responses to water stress, I. Scope and
28 general outline, *Adv. Water Resour.*, 24, 695–705, 2001.

29 Rosenzweig, C. and Abramopoulos, F.: Land-surface model development for the GISS GCM,
30 *J. Climate*, 10, 2040–2054, 1997.

1 Sala, A., Woodruff, D. R., and Meinzer, F. C.: Carbon dynamics in trees: feast or famine?,
2 *Tree Physiol.*, 32, 764–775, 2012.

3 Schmid, H. P., Grimmond, C. S. B., Cropley, F., Offerle, B., and Su, H. B.: Measurements of
4 CO₂ and energy fluxes over a mixed hardwood forest in the mid-western United States, *Agr.*
5 *Forest Meteorol.*, 103, 357–374, 2000.

6 Schmidt, G. A., Ruedy, R., Hansen, J. E., Aleinov, I., Bell, N., Bauer, M., Bauer, S., Cairns,
7 B., Canuto, V., Cheng, Y., Del Genio, A., Faluvegi, G., Friend, A. D., Hall, T. M., Hu, Y.,
8 Kelley, M., Kiang, N. Y., Koch, D., Lacis, A. A., Lerner, J., Lo, K. K., Miller, R. L.,
9 Nazarenko, L., Oinas, V., Perlwitz, J. P., Perlwitz, J., Rind, D., Romanou, A., Russell, G. L.,
10 Sato, M., Shindell, D. T., Stone, P. H., Sun, S., Tausnev, N., Thresher, D., and Yao, M.-S.:
11 Present day atmospheric simulations using GISS ModelE: comparison to in-situ, satellite and
12 reanalysis data, *J. Climate*, 19, 153–192, doi:10.1175/JCLI3612.1, 2006.

13 Schmidt, G. A., Kelley, M., Nazarenko, L., Ruedy, R., Russell, G. L., Aleinov, I., Bauer, M.,
14 Bauer, S. E., Bhat, M. K., Bleck, R., Canuto, V., Chen, Y.-H., Cheng, Y., Clune, T. L., Del
15 Genio, A., de Fainchtein, R., Faluvegi, G., Hansen, J. E., Healy, R. J., Kiang, N. Y., Koch, D.,
16 Lacis, A. A., LeGrande, A. N., Lerner, J., Lo, K. K., Matthews, E. E., Menon, S., Miller, R.
17 L., Oinas, V., Oloso, A. O., Perlwitz, J. P., Puma, M. J., Putman, W. M., Rind, D., Romanou,
18 A., Sato, M., Shindell, D. T., Sun, S., Syed, R. A., Tausnev, N., Tsigaridis, K., Unger, N.,
19 Voulgarakis, A., Yao, M.-S., and Zhang, J.: Configuration and assessment of the GISS
20 ModelE2 contributions to the CMIP5 archive, *J. Adv. Model. Earth Syst.*, 6, 141–184, 2014.

21 Schneider, R., Berninger, F., Ung, C. H., Makela, A., Swift, D. E., and Zhang, S. Y., Within
22 crown variation in the relationship between foliage biomass and sapwood area in jack pine,
23 *Tree Physiol.*, 31, 22–29, 2011.

24 Sitch, S., Smith, B., Prentice, I.C., Arneeth, A., Bondeau, A., Cramer, W., Kaplan, J., Levis, S.,
25 Lucht, W., Sykes, M., Thonicke, K., and Venevsky, S: Evaluation of ecosystem dynamics,
26 plant geography and terrestrial carbon cycling in the LPJ dynamic global vegetation model,
27 *Glob. Change Biol.*, 9, 161–185, 2003.

28 Stephens, B. B., Gurney, K. R., Tans, P. P., Sweeney, C., Peters, W., Bruhwiler, L., Ciais, P.,
29 Ramonet, M., Bousquet, P., Nakazawa, T., Aoki, S., Machida, T., Inoue, G., Vinnichenko, N.,
30 Lloyd, J., Jordan, A., Heimann, M., Shibistova, O., Langenfelds, R., Steele, L. P., Francey, T.,

1 and Denning, A. S.: Weak northern and strong tropical land carbon uptake from vertical
2 profiles of atmospheric CO₂, *Science*, 316, 1732–1735, 2007.

3 Stöckli, R. and Vidale, P. L.: European plant phenology and climate as seen in a 20 year
4 AVHRR land-surface parameter dataset, *Int. J. Remote Sens.*, 25, 3303–3330, 2004.

5 Stöckli, R., Lawrence, D. M., Niu, G.-Y., Oleson, K. W., Thornton, P. E., Yang, Z.-L.,
6 Bonan, G. B., Denning, A. S., and Running, S. W.: Use of FLUXNET in the community land
7 model development, *J. Geophys. Res.-Biogeo.*, 113, G01025, doi:10.1029/2007JG000562,
8 2008.

9 Stöckli, R., Rutishauser, T., Baker, I., Liniger, M. A., and Denning, A. S.: A global reanalysis
10 of vegetation phenology, *J. Geophys. Res.-Biogeo.*, 116, G03020,
11 doi:10.1029/2010JG001545, 2011.

12 Tang, J. W. and Baldocchi, D. D.: Spatial–temporal variation in soil respiration in an oak-
13 grass savanna ecosystem in California and its partitioning into autotrophic and heterotrophic
14 components, *Biogeochemistry*, 73, 183–207, 2005.

15 Tang, J. W., Baldocchi, D. D., and Xu, L.: Tree photosynthesis modulates soil respiration on a
16 diurnal time scale, *Glob. Change Biol.*, 11, 1298–1304, 2005.

17 Thompson, M. V., Randerson, J. T., Malmström, C. M., and Field, C. B.: Change in net
18 primary production and heterotrophic respiration: How much is necessary to sustain the
19 terrestrial carbon sink?, *Global Biogeochemical Cycles*, 10, 711–726, 1996.

20 Urbanski, S., Barford, C., Wofsy, S., Kucharik, C., Pyle, E., Budney, J., McKain, K., Fitz
21 jarrald, D., Czikowsky, M., and Munger, J. W.: Factors controlling CO₂ exchange on
22 timescales from hourly to decadal at Harvard Forest, *J. Geophys. Res.-Biogeo.*, 112, G02020,
23 doi:10.1029/2006JG000293, 2007.

24 van der Tol, C., Berry, J. A., Campbell, P. K. E., and Rascher, U.: Models of fluorescence and
25 photosynthesis for interpreting measurements of solar-induced chlorophyll fluorescence, *J.*
26 *Geophys. Res.-Biogeo.*, 119, 2312–2327, 2014.

27 Wang, Y. P., Baldocchi, D., Leuning, R., Falge, E., and Vesala, T.: Estimating parameters in a
28 land-surface model by applying nonlinear inversion to eddy covariance flux measurements
29 from eight FLUXNET sites, *Glob. Change Biol.*, 13, 652–670, 2007.

1 Wei, J., Dickinson, R. E., and Zeng, N.: Climate variability in a simple model of warm
2 climate land–atmosphere interaction, *J. Geophys. Res.-Biogeo.*, 111, G03009,
3 doi:10.1029/2005JG000096, 2006.

4 Welp, L. R., Keeling, R. F., Meijer, H. A. J., Bollenbacher, A. F., Piper, S. C., Yoshimura, K.,
5 Francey, R. J., Allison, C. E., and Wahlen, M.: Interannual variability in the oxygen isotopes
6 of atmospheric CO₂ driven by El Niño, *Nature*, 477, 579–582, 2011.

7 White, M. A., Thornton, P. E., and Running, S. W.: A continental phenology model for
8 monitoring vegetation responses to interannual climatic variability, *Global Biogeochem. Cy.*,
9 11, 217–234, 1997.

10 Wilson, K., Goldstein, A., Falge, E., Aubinet, M., Baldocchi, M., Berbigier, P., Bernhofer, C.,
11 Ceulemans, R., Dolman, H., Field, C., Grelle, A., Ibrom, A., Law, B. E., Kowalski, A.,
12 Meyers, T., Moncrieff, J., Monson, R., Oechel, W., Tenhunen, J., Verma, S., and Valentini,
13 R.: Energy balance closure at FLUXNET sites, *Agr. Forest Meteorol.*, 113, 223–243, 2002.

14 Xu, L. and Baldocchi, D. D.: Seasonal variation in carbon dioxide exchange over a
15 Mediterranean annual grassland in California, *Agr. Forest Meteorol.*, 123, 79–96, 2004.

16 Xue, Y. K., Fennessy, M. J., and Sellers, P. J.: Impact of vegetation properties on US summer
17 weather prediction, *J. Geophys. Res.-Atmos.*, 101, 7419–7430, 1996.

18 Yang, W., Ni-Meister, W., Kiang, N. Y., Moorcroft, P. R., Strahler, A. H., and Oliphant, A.:
19 A clumped-foliage canopy radiative transfer model for a Global Dynamic Terrestrial
20 Ecosystem Model II: comparison to measurements, *Agr. Forest Meteorol.*, 150, 895–907,
21 2010.

22 Zhang, X. Y., Tarpley, D., and Sullivan, J. T.: Diverse responses of vegetation phenology to a
23 warming climate, *Geophys. Res. Lett.*, 34, L19405, doi:10.1029/2007GL031447, 2007.

24
25
26

1 Table 1. Plant Functional Types (PFT) in Ent.

Number	Plant Function Type
1	Evergreen broadleaf early successional
2	Evergreen broadleaf late successional
3	Evergreen needleleaf early successional
4	Evergreen needleleaf late successional
5	Cold deciduous broadleaf early successional
6	Cold deciduous broadleaf late successional
7	Drought deciduous broadleaf
8	Deciduous needleleaf
9	Cold adapted shrub
10	Arid adapted shrub
11	C3 grass perennial
12	C4 grass
13	C3 grass annual
14	Arctic C3 grass
15	C3 crops
16	C4 crops
17	Crops broadleaf woody

2

3

1 Table 2. Parameters in phenology submodel.

Parameters	Values	Eq. #	References
GDD_{int}	-68		
GDD_{stop}	638	(3)	Botta et al. (2000)
GDD_{multi}	-0.01		
GDD_{length}	200	(4)	Derived from observations at MMSF
T_{max}	15		
T_{min}	5	(5)	Adjusted based on Jolly et al. (2005)
ld_{max}	540		
ld_{max}	660		
$SGDD_{crit}$	100 for arctic C3 grass; 400 for C3 grass; 1400 for C4 grass;	(6)	Arctic C3 grass derived from observations at Barrow, AK C3 annual grass from White et al. (1997)
$SGDD_{length}$	50		
TS_{max}	0	(7)	Derived from observations at Tonzi and Vaira
TS_{min}	-5		
β_{max}	0.4 for both woody and herbaceous	(8)	Derived from observations at Tonzi
β_{min}	0.0 for woody; 0.2 for herbaceous		
β_{resis}	0.25 for woody; 1.0 for herbaceous		
a	1	(9)	
b	0		
τ	125 hr	(10)	Makela et al. (2006)
T_0	-5.9°C		
$S_{h,max}$	16.8°C	(11)	Derived from observations at Hyytiala

2

3

4

Table 3. Site descriptions.

	Morgan Monroe State Forest	Harvard Forest	Vaira Ranch	Tonzi Ranch	Hyytiala
Short name	MMS	Ha1	Var	Ton	Hyy
Location	Indiana, USA	Massachusetts, USA	California, USA	California, USA	Hyytiala, Finland
Coordinates	39.32°N, 86.41°W	42.54°N, 72.17°W	38.41°N, 120.95°W	38.43°N, 120.97°W	61.85°N, 24.29°W
Primary reference	Schmid et al. (2000)	Urbanski et al. (2007)	Xu and Baldocchi (2004)	Baldocchi et al. (2004)	Makela et al. (2004)
Data website	http://ameriflux.ornl.gov/fullsiteinfo.php?sid=48	http://ameriflux.ornl.gov/fullsiteinfo.php?sid=50	http://ameriflux.ornl.gov/fullsiteinfo.php?sid=30	http://ameriflux.ornl.gov/fullsiteinfo.php?sid=29	1.1 http://gaia.agraria.unitus.it/home/site-details?id=117
Dominant Species	Sugar maple, Tulip poplar	Red oak, Red maple	Purple false brome	Overstory: Blue oak, Understory: Purple false brome	Scots pine, Norway spruce
Ent PFT	6-cold deciduous broadleaf l.s.	5-cold deciduous broadleaf e.s.	13-annual grass	7-drought deciduous Broadleaf & 13-annual grass	4-evergreen needleleaf
Simulation Period	1 Jan 2002 – 31Dec 2006	1 Jan 1994 – 31Dec 2002	1 Jan 2002 – 31Dec 2002	1 Jan 2002 – 31Dec 2002	1 Jan 1998 – 31Dec 1998
Experiments	LSM-oveg	LSM-oveg	Ent-oveg	Ent-oveg	Ent-oveg
	LSM-dveg	LSM-dveg	LSM-oveg	LSM-oveg	LSM-oveg
			LSM-dveg	LSM-dveg	LSM-dveg

Table 4. Types of experiments.

	Soil state (moisture and temperature)	Vegetation phenology
Ent-dveg	Prescribed with observation (Ent-standalone)	Prognostic LAI (dynamic “active biomass” phenology)
Ent-oveg	Prescribed with observation (Ent-standalone)	Prescribed with observed LAI
LSM-dveg	Prognostic (Ent-LSM coupled)	Prognostic LAI
LSM-oveg	Prognostic (Ent-LSM coupled)	Prescribed with observed LAI

Table 5. Correlation coefficients and RMSEs of LAI-based phenological dates between simulations and observations.

Site	Spring Phenology						Fall Phenology					
	20% LAI		50% LAI		80% LAI		80% LAI		50% LAI		20% LAI	
	R	RMSE	R	RMSE	R	RMSE	R	RMSE	R	RMSE	R	RMSE
MMS (2002-2006)	0.80	3.65	0.36	6.75	0.67	16.44	0.20	27.95	0.46	19.65	0.49	7.67
Ha1 (1994-2002)	0.44	5.71	0.85	3.00	0.44	9.18	0.55	9.91	0.04	15.09	-0.56	17.52

Table 6. Correlation coefficients and RMSEs of hourly and daily fluxes between simulations and observations.

Site	Years		NEP ($\mu\text{mol}/\text{m}^2/\text{s}$)				ET (mm/s)			
			Hourly		Daily		Hourly		Daily	
			R	RMSE	R	RMSE	R	RMSE	R	RMSE
MMS	2002	LSM-dveg	0.86	3.67	0.91	1.31	0.80	67.89	0.85	32.82
	-2006	LSM-oveg	0.88	3.59	0.94	1.04	0.79	66.62	0.85	32.12
Ha1	1994	LSM-dveg	0.89	3.03	0.85	1.70	0.79	45.25	0.82	22.46
	-2002	LSM-oveg	0.92	2.72	0.92	1.36	0.74	52.12	0.72	29.14
Var	2002	Ent-dveg	0.74	2.92	0.57	1.41	-	-	-	-
		Ent-oveg	0.76	2.81	0.55	1.60	-	-	-	-
		LSM-dveg	0.70	2.57	0.75	1.16	0.84	25.37	0.83	13.46
		LSM-oveg	0.84	2.34	0.72	1.54	0.91	25.73	0.93	11.36
Ton	2002	Ent-dveg	0.42	3.96	0.36	1.51	-	-	-	-
		Ent-oveg	0.44	3.94	0.43	1.50	-	-	-	-
		LSM-dveg	0.41	4.06	0.53	1.37	0.77	5.38	0.83	14.42
		LSM-oveg	0.42	3.99	0.50	1.41	0.76	35.59	0.84	14.40
Hyy	1998	Ent-dveg	0.79	2.63	0.71	1.25	-	-	-	-
		Ent-oveg	0.77	2.90	0.68	1.35	-	-	-	-
		LSM-dveg	0.92	1.66	0.86	0.82	0.87	19.37	0.93	7.89
		LSM-oveg	0.90	1.89	0.82	0.92	0.87	19.30	0.94	7.88

Appendix Table A1. Plant functional type parameters for root density distributions.

Ent plant functional type																
	Evergreen broad		Evergreen needle		Cold-deciduous broad		drought broad	decidciduous needle	shrub cold	shrub arid	grass				crop herb	crop tree
PET	1	2	3	4	5	6	7	8	9	10	11	12	13	14	15	16
a	1.1	1.1	0.25	0.25	0.25	0.25	0.25	0.25	0.8	0.8	0.9	0.9	0.9	0.9	0.9	0.25
b	0.4	0.4	2.0	2.0	2.0	2.0	2.0	2.0	0.4	0.4	0.9	0.9	0.9	0.9	0.9	2.0

- 1 Appendix Table B1. Values of C pool parameters: cnratio – C:N ratio of all 12 C pools (used
 2 only to calculate N pools); $\text{annk}_{\text{soil}}$ – inverse of turnover times of all 9 soil C pools (yr^{-1}).

Pool	C:N ratio ¹	$\text{annk}_{\text{soil}}$ ²	~turnover time
Leaf	30	--	(lage) See
Root	130	--	(lage)
Wood	55	--	(woodage)
Surfmet	30	14.8	25 d
Surfstr	50	3.9	94 d
Soilmet	25	18.5	20 d
Soilstr	50	4.9	74 d
CWD	135	0.2424	4.1 yr
Surfmic	12.5	6	60 d
Soilmic	12.5	7.3	50 d
Slow	12.5	0.2	5 yr
Passive	8.5	0.002	500 yr

3 ¹from original CASA code (Potter et al., 1993)

4 ²from CASA' code (Doney et al., 2006)

1 Appendix Table B2. Values of respiration pathway coefficients: eff – microbial respiration
 2 transfer efficiencies for all 14 pathways; frac_donor – additional respiration efficiencies (both
 3 unitless)

Pathway	eff ¹	frac_donor ²
1	0.45	0.003+(0.009*clay frac)
2	0.45	1-frac_donor(1)
3	0.4	1
4	0.4	1-structurallignin(PFT) ³
5	0.7	structurallignin(PFT)
6	0.45	1
7	0.45	1-structurallignin(PFT)
8	0.7	structurallignin(PFT)
9	0.4	1-woodligninfrac ³
10	0.7	woodligninfrac
11	0.4	1
12	0.85-[0.68* (silt+sand fracs)]	0.003+(0.032*clay frac)
13	0.85-[0.68* (silt+sand fracs)]	1-frac_donor(12)
14	0.45	1

4 ¹from CASA code (Potter et al., 1993) for 1–3, others from CASA' code
 5 (Doney et al., 2006) ****double check which from which code****

6 ²from original CASA code (Potter et al., 1993)

7 ³derived litter coefficients in both CASA and CASA' codes

8

1 Appendix Table D1. Biophysics parameters for Fluxnet sites in this study.

Variable	Definition	Unit	PFT4	PFT5	PFT6	PFT7	PFT13
			Hyy	Ha1	MMS	Ton (oak)	Var & Ton (grass)
P_{st}	Pst - photosynthetic pathway	-	C3	C3	C3	C3	C3
PAR_{absorb}	Leaf PAR absorbance	-	0.93	0.90	0.90	0.90	0.86
V_{cmax}^1	Maximum photosynthetic capacity	$\mu\text{mol m}^{-2} \text{s}^{-1}$	43.0 ²	60.0 ²	51.0 ³	56.4 ⁴	50.1 ⁴
m	Slope of Ball-Berry stomatal conductance equations	-	9.0	9.0	9.0	9.0	11.0
b	Intercept of Ball-Berry stomatal conductance equation	$\mu\text{mol m}^{-2} \text{s}^{-1}$	0.002	0.002	0.002	0.002	0.008

2 ¹For all these plant functional types there is a large range of values, as well as large variation within a single site and single plant. We
3 therefore have chosen literature values for the Fluxnet sites where available, and tuned the value within the literature range for the site.

4 ²Oleson et al. (2004)

5 ³Wilson et al. (2001)

6 ⁴Wang et al. (2007)

7

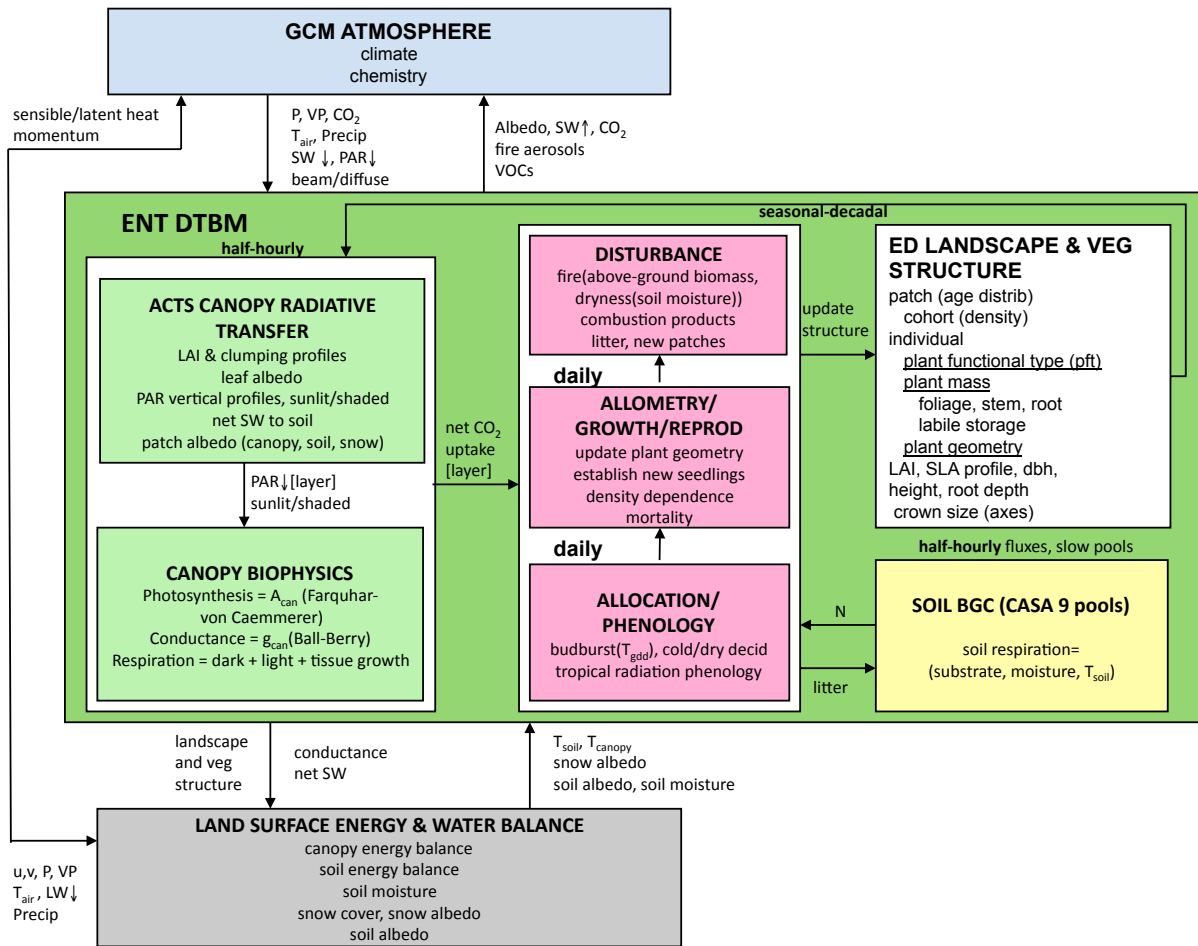
8

9

1 Appendix Table D2. Biogeochemical and phenological parameters for Fluxnet sites in this study.

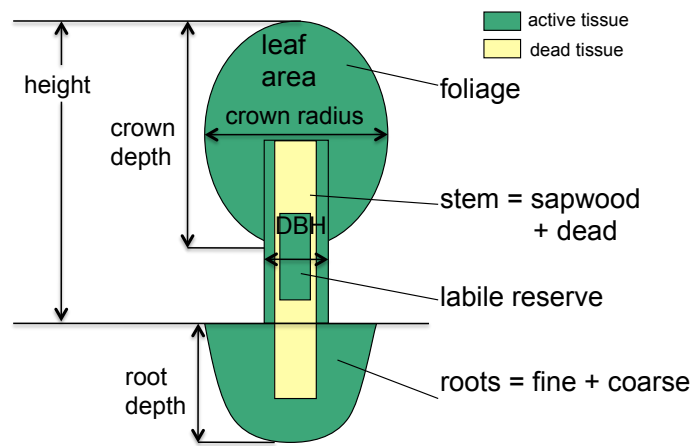
Variable	Defintion	Unit	PFT4	PFT5	PFT6	PFT7	PFT13
			Hyy	Ha1	MMS	Ton (oak)	Var & Ton (grass)
leaftype	Leaf type	-	needle	broad	broad	broad	grass
h _{wilt}	Wilting point	m	-153.0	-500.0	-500.0	-500.0	-2030.0
S*	Soil moisture stress onset point (fraction of soil volumetric saturation)	-	0.50	0.50	50.0	0.34	0.65
s _{wilt}	Wilting point (fraction of soil volumetric saturation)	-	0.25	0.29	0.29	0.28	0.27
sla	Specific leaf area	m ² _{leaf} /kgC _{leaf}	9.5	34.5	34.0	8.3	21.6
r	Respiration parameter	-	1.2	0.6	0.6	0.5	1.2
l _{rage}	Leaf and root litter age	years	4.0	1.2	0.75	1.2	1.5
woodage	Stem litter age	years	42.0	58.0	58.0	245.0	UNDEF
lit_C2N	Litter C:N ratio	-	80.0	57.0	57.0	60.0	50.0
lignin	Lignin content	-	0.25	0.2	0.3	0.2	0.1
croot_ratio	Coarse roots:woody stem mass ratio	-	0.184	0.093	0.093	0.153	0.0
phenotype	Phenological type	-	Cold deciduous	Cold deciduous	Cold deciduous	Drought deciduous	Annual
b1Cf	Parameter 1 for allometric relation between DBH and foliage carbon	-	0.045	0.024	0.017	0.0296	0.0800
b2Cf	Parameter 2 for allometric relation between DBH	-	1.683	1.860	1.731	1.560	1.000

	and foliage carbon						
b1Cd	Parameter 1 for allometric relation between DBH and structural carbon	-	0.1617	0.148	0.235	0.0621	0.00001
b2Cd	Parameter 2 for allometric relation between DBH and structural carbon	-	2.1536	2.411	2.252	2.306	1.000
b1Ht	Parameter 1 for allometric relation between DBH and height	-	22.79	25.18	23.39	34.62	0.4778
b2Ht	Parameter 2 for allometric relation between DBH and height	-	-0.0445	-0.0496	-0.054	-0.02321	-0.75



1
2
3

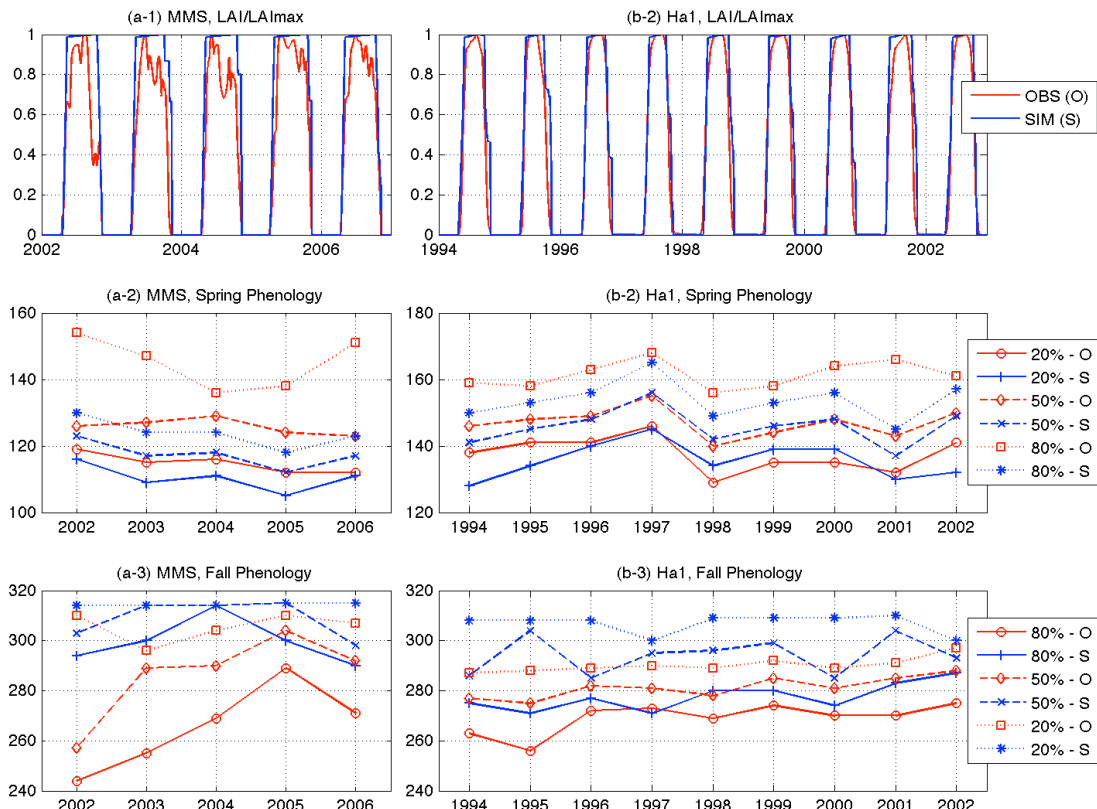
Figure 1. Schematic diagram of the Ent model.



1

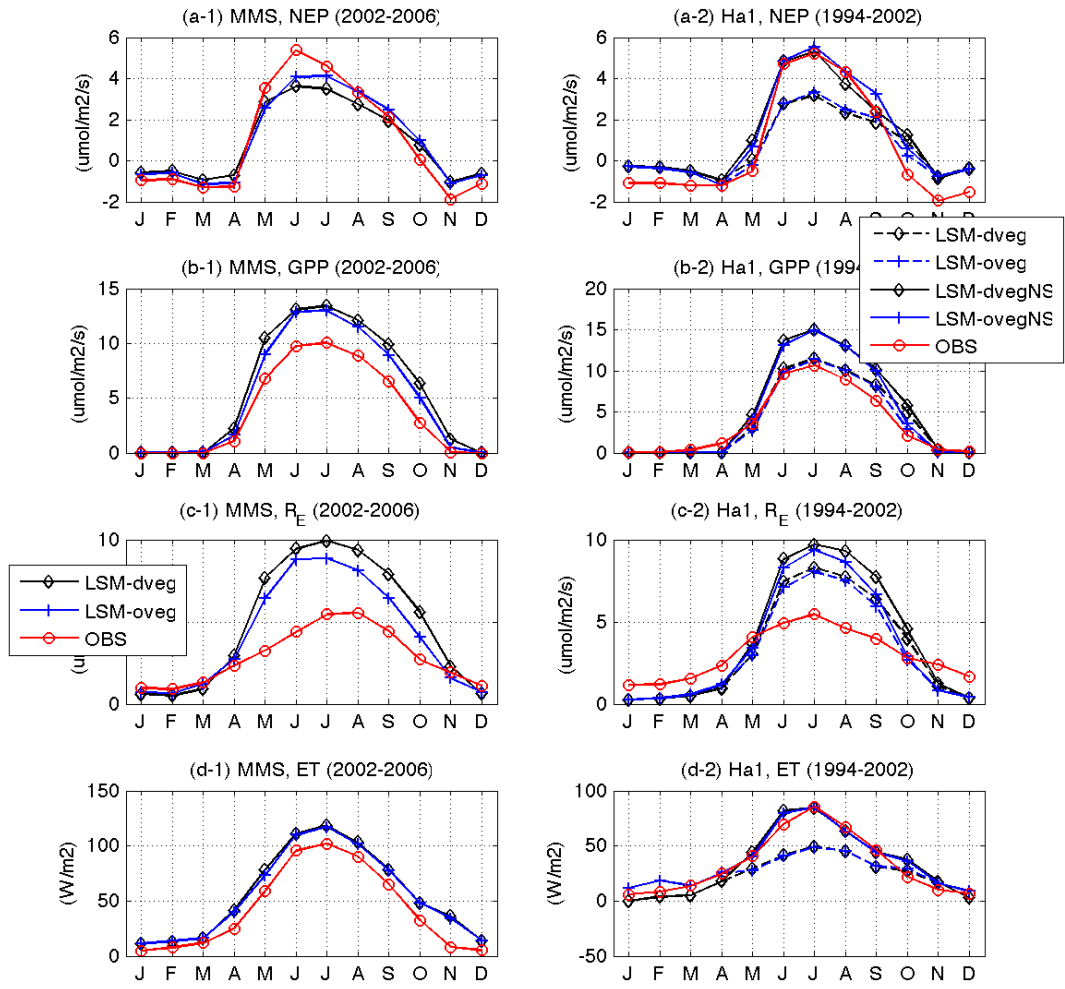
2 Figure 2. Ent individual plant biomass pools and geometry. Herbaceous plants exclude
 3 woody tissue.

4



1
2
3
4
5
6
7
8
9

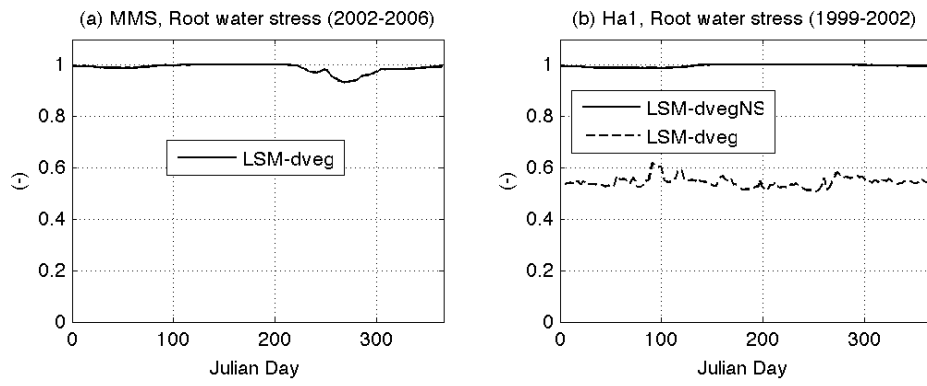
Figure 3. Daily simulated (S) and observed (O) phenology: (top) LAI/LAI_{max} (middle) phenological dates (day of year) for spring leaf-out at percent of maximum; and (bottom) phenological dates (day of year) for fall senescence in MMSF and Harvard Forest. These results show good simulated timing of initial leaf-out and final senescence, but lack of the gradual rate of these, such that maximum leaf-out occurs too soon, and period of peak growth is too long. The gradual behavior could be simulated through a rate constraint.



1

2 Figure 4. Average monthly fluxes in MMSF for 2002-2006 and Harvard Forest for 1994-
 3 2002: (a) NEP, (b) GPP, (c) R_E and (d) ET.

4

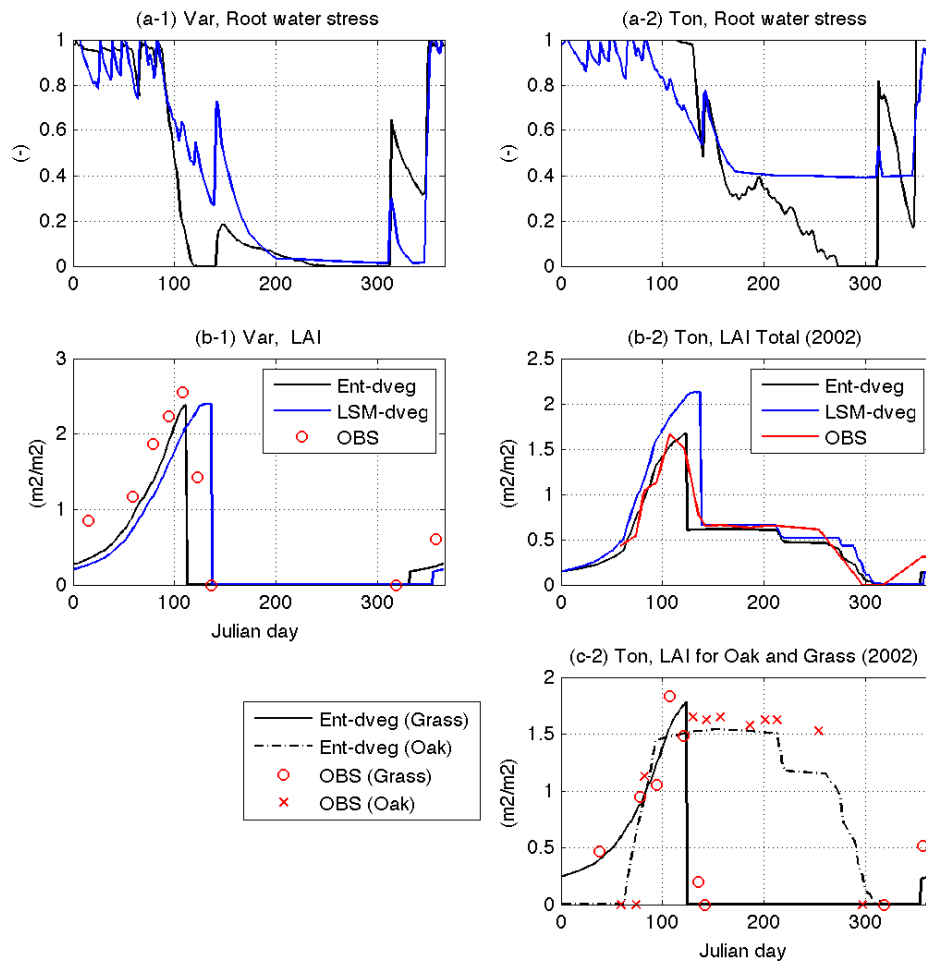


1

2

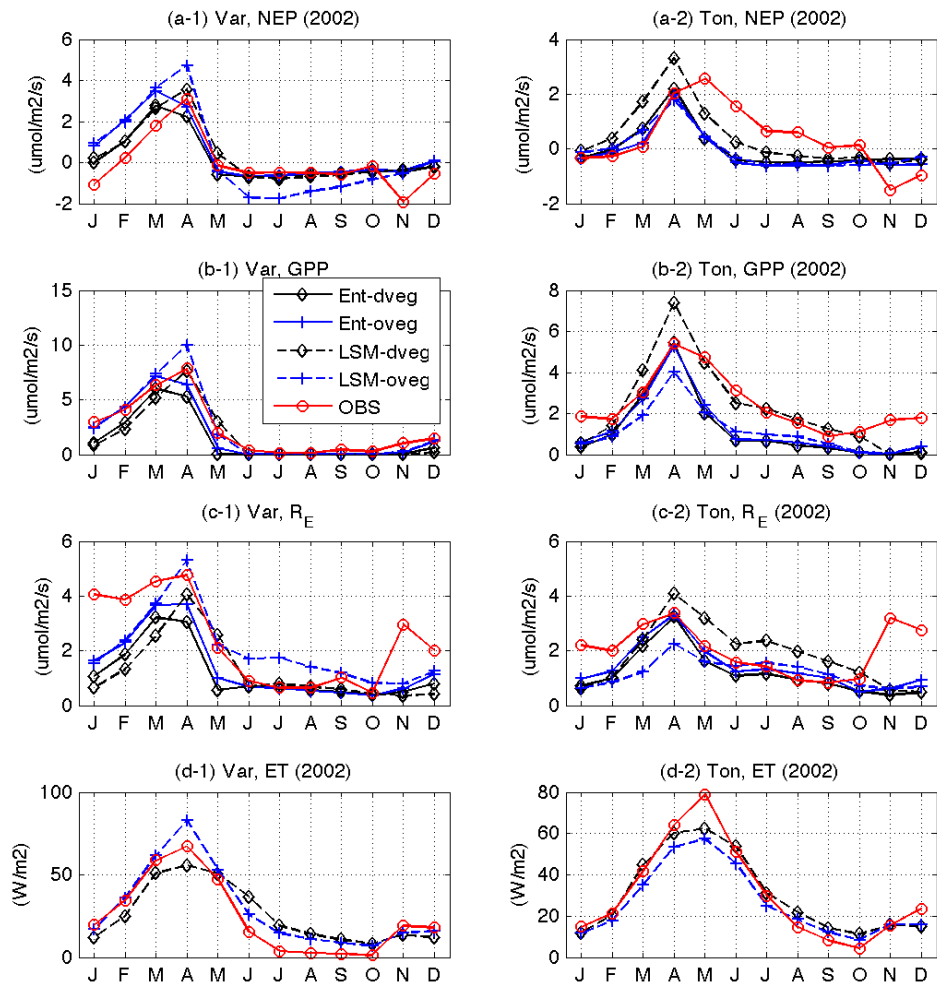
3 Figure 5. Daily root water stress factor in (a) MMSF for 2002-2006 and (b) Harvard Forest
 4 for 1994-2002.

5



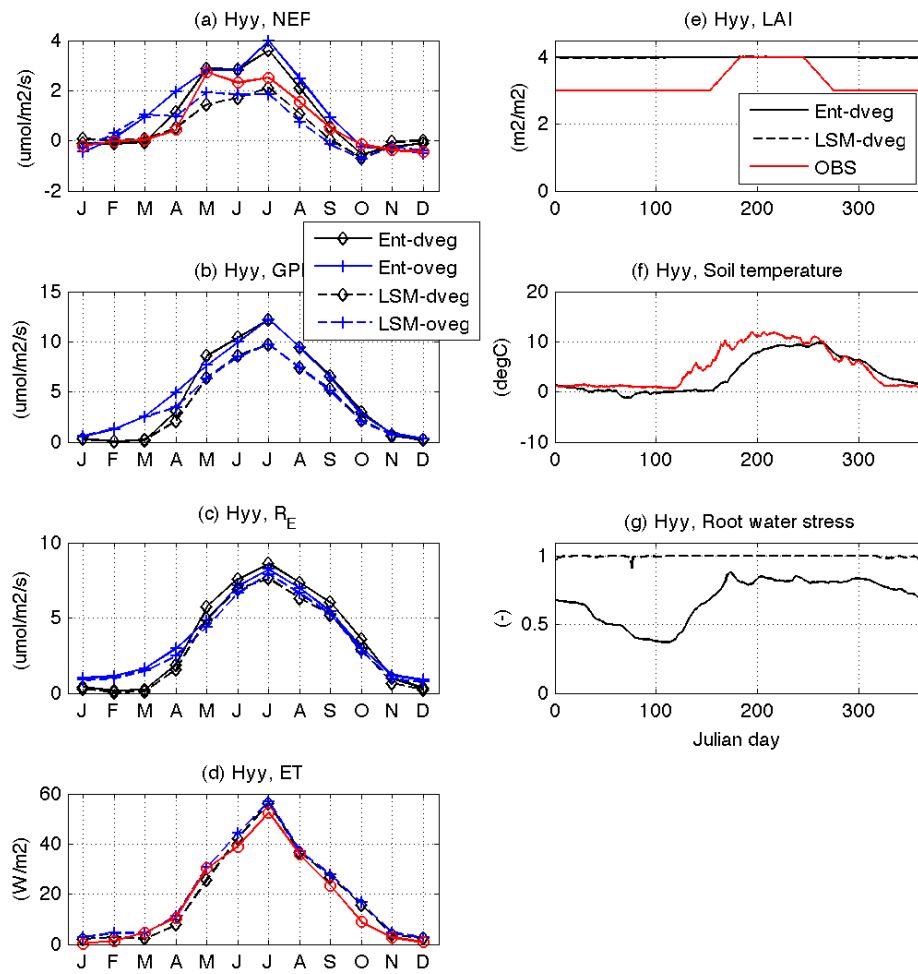
1
2
3
4
5

Figure 6. (a) Daily root water stress and (b-c) daily LAI in Vaira and Tonzi Ranches for 2002.



1
2
3
4
5

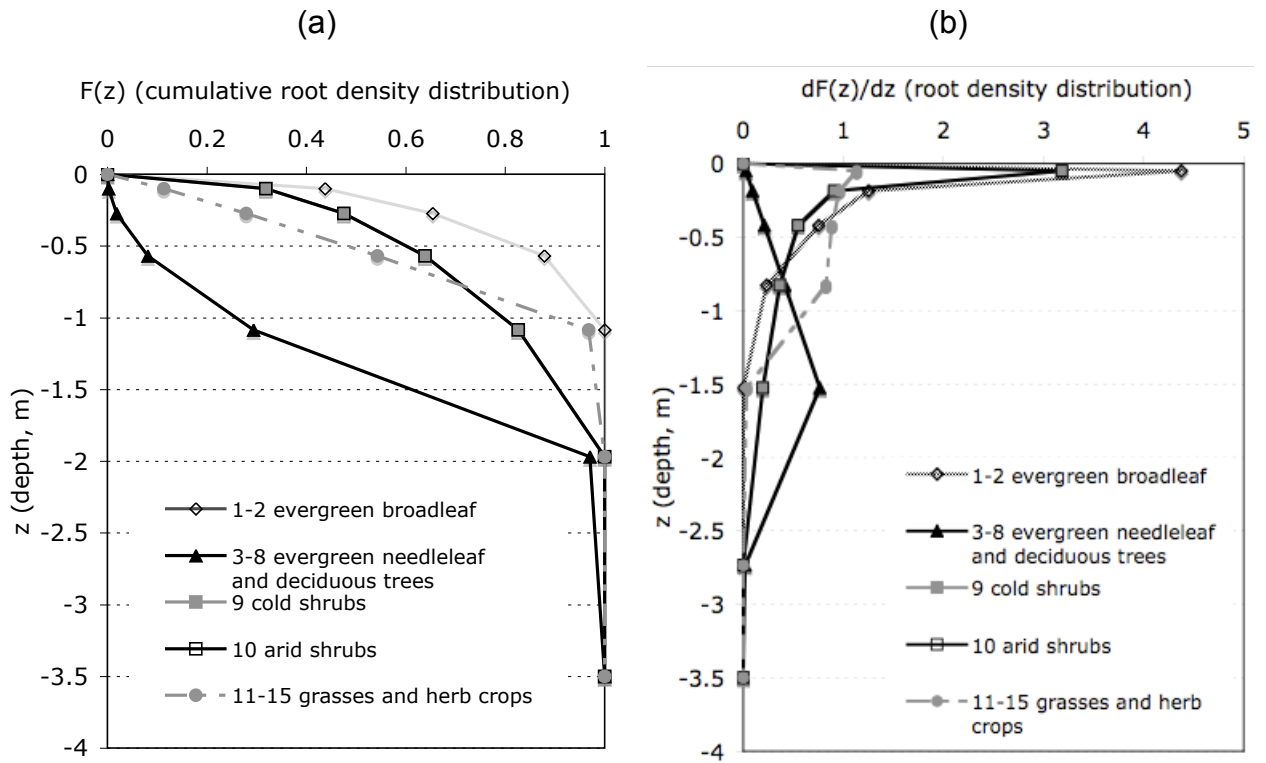
Figure 7. Monthly fluxes in Vaira and Tonzi Ranches for 2002: (a) NEP, (b) GPP, (c) R_E and (d) ET.



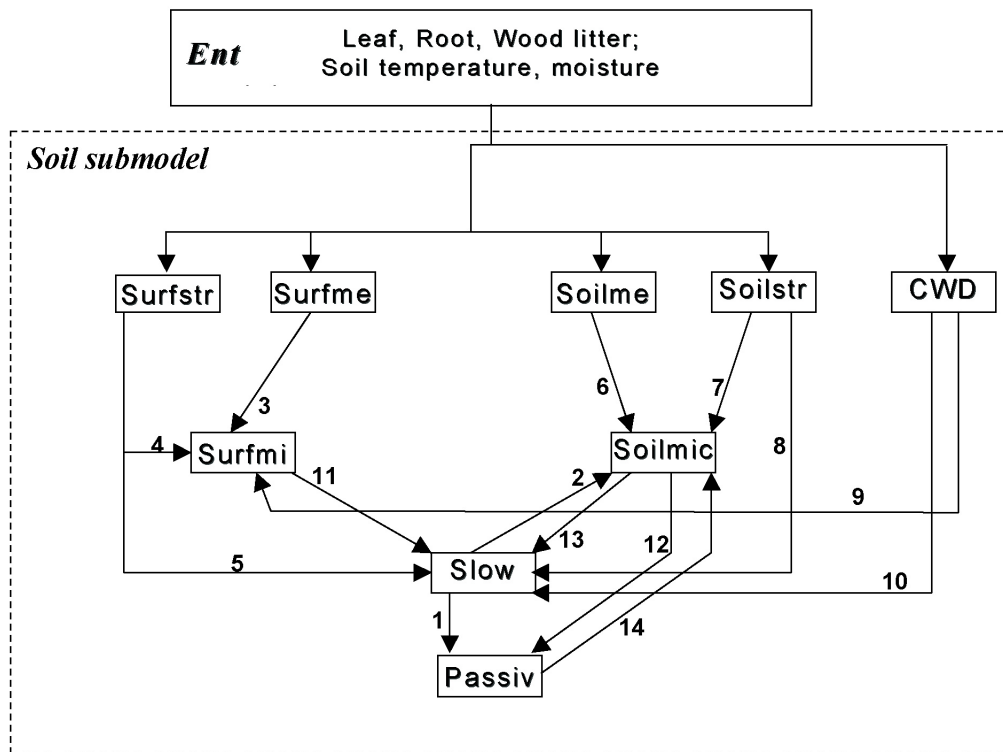
1
2
3
4
5
6

Figure 8. Monthly fluxes and daily states in Hyytiala for 1998: (a) NEP, (b) GPP, (c) RE, (d) ET, (e) LAI, (f) soil temperature and (g) root water stress. Here the observed LAI is assumed based on personal communication with the site investigator, Pasi Kolari.

1



2 Appendix Figure A1. (a) Cumulative root density profile distributions and (b) probability
3 density distributions in the EntTBM, modified from (Rosenzweig and Abramopoulos 1997),
4 by soil depth increments of the NASA GISS GCM land surface model.
5

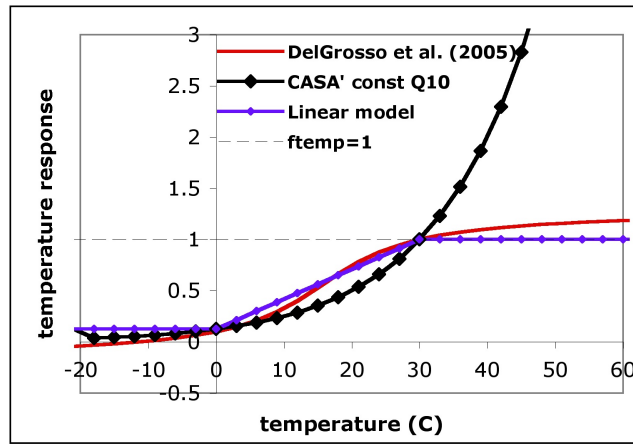


1

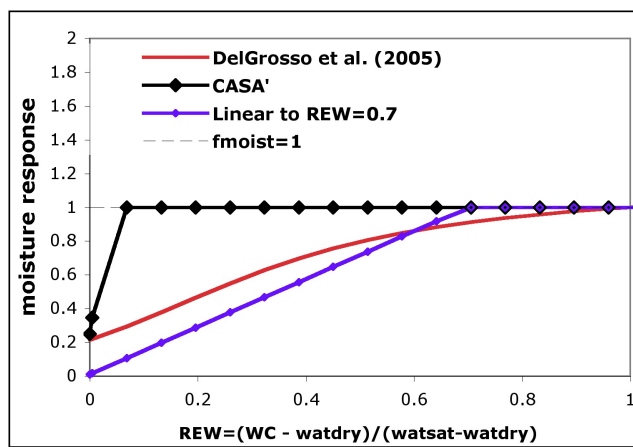
2 Appendix Figure B1. Schematic diagram of soil biogeochemistry submodel of Ent (showing 9
 3 soil C pools only; modified from Potter et al., 1993). Surfstr – surface structural pool; Surfmet
 4 – surface metabolic pool; Soilmet – soil metabolic pool (fastest to decompose; 20-day
 5 turnover time); Soilstr – soil structural pool; Surfmic – surface microbial pool; Soilmic – soil
 6 microbial pool; Slow – slowly decomposing pool; Passiv – very slowly decomposing pool
 7 (500-yr turnover time). All pools except for the 3 surf*** pools are assumed to be present in
 8 the 2 lower soil layers in addition to the top layer.

9

(a)



(b)



1

2 Appendix Figure B2. (a) Temperature responses of soil respiration in Del Grosso et al.
3 (2005), CASA', and Ent's piece-wise linear response and (b) moisture response of soil
4 respiration in Del Grosso et al. (2005), CASA', and Ent for grassland (Vaira Ranch) soil
5 texture.